Article

Targeting symbionts by apolipoprotein L proteins modulates gut immunity

https://doi.org/10.1038/s41586-025-08990-4

Received: 4 June 2024

Accepted: 7 April 2025

Published online: 14 May 2025

Check for updates

Tao Yang[1,8], Xiaohu Hu[1,8], Fei Cao[2,8], Fenglin Yun[1], Kaiwen Jia[3], Mingxiang Zhang[4], Gaohui Kong[1], Biyu Nie[1], Yuexing Liu[1], Haohao Zhang[2], Xiaoyu Li[5], Hongyan Gao[6], Jiantao Shi[3], Guanxiang Liang[6], Guohong Hu[1], Dennis L. Kasper[7], Xinyang Song[2]✉ & Youcun Qian[1,4]✉

The mammalian gut harbours trillions of commensal bacteria that interact with their hosts through various bioactive molecules[1,2]. However, the mutualistic strategies that hosts evolve to benefit from these symbiotic relationships are largely unexplored. Here we report that mouse enterocytes secrete apolipoprotein L9a and b (APOL9a/b) in the presence of microbiota. By integrating flow cytometry sorting of APOL9-binding bacterial taxa with 16S ribosomal RNA gene sequencing (APOL9-seq), we identify that APOL9a/b, as well as their human equivalent APOL2, coat gut bacteria belonging to the order of Bacteroidales with a high degree of specificity through commensal ceramide-1-phosphate (Cer1P) lipids. Genetic abolition of ceramide-1-phosphate synthesis pathways in gut-dominant symbiote *Bacteroides thetaiotaomicron* significantly decreases the binding of APOL9a/b to the bacterium. Instead of lysing the bacterial cells, coating of APOL9a/b induces the production of outer membrane vesicles (OMVs) from the target bacteria. Subsequently, the *Bacteroides*-elicited outer membrane vesicles enhance the host's interferon-γ signalling to promote major histocompatibility complex class II expression in the intestinal epithelial cells. In mice, the loss of *Apol9a/b* compromises the gut major histocompatibility complex class II-instructed immune barrier function, leading to early mortality from infection by intestinal pathogens. Our data show how a host-elicited factor benefits gut immunological homeostasis by selectively targeting commensal ceramide molecules.

The microorganisms inhabiting the mammalian gut live in symbiosis with their host. These microorganisms facilitate nutrient absorption and metabolism, as well as directing the development of the host immune system through various metabolites or structural molecules they produce. For instance, short-chain fatty acids or bile acids produced by microorganisms induce the differentiation of regulatory T (T_{reg}) cells in the colonic lamina propria[3–8], whereas indole derivatives and linoleic acid isomers derived from microorganisms promote the accumulation of $CD4^+CD8\alpha\alpha^+$ intraepithelial lymphocytes (IELs) in the small intestine[9,10]. Microbial membrane-associated molecules, such as polysaccharide A and α-galactosylceramides derived from the human symbiont *Bacteroides fragilis*, have also been shown to have immunomodulatory activities on colonic T_{reg} cells and natural killer T cells, respectively[11,12].

As the intestinal immune system matures, it develops sophisticated defence mechanisms to cope with various immunological challenges from both endogenous microbiota and invading pathogens. The intestinal epithelial barrier is coated with glycosylated mucins to form a gel-like protective layer that contains antimicrobial proteins (AMPs) produced by specialized intestinal epithelial cells (IECs) or secretory antibodies from intestinal plasma cells[13,14]. Recently, it has been discovered that stromal cells associated with intestinal lymphoid follicles secrete complement component 3 (C3) into the intestinal lumen for bacterial deposition and pathogen clearance[15]. The binding of these intestinal defence factors to certain microbial species belonging to either Gram-positive or Gram-negative species allows them to segregate symbionts from the mucosal surface, thereby maintaining host–microbiota mutualistic interactions[16–22]. However, their targeting specificities do not seem to exhibit a phylogenetic preference. It is therefore of interest to investigate whether the host can evolve tactics to selectively target specific members of a complex microbial consortium, and how this immune–microbial mutualism benefits the development and functionality of the intestinal immune system.

Gut enterocytes produce apolipoprotein L9a/b

Previous studies have demonstrated that microbial colonization induces transcriptional changes in the ileal IECs of the host[16,23]. To further

[1]Shanghai Institute of Nutrition and Health, University of Chinese Academy of Sciences, Chinese Academy of Sciences, Shanghai, China. [2]Key Laboratory of Multi-Cell Systems, Shanghai Institute of Biochemistry and Cell Biology, Center for Excellence in Molecular Cell Science, Chinese Academy of Sciences, University of Chinese Academy of Sciences, Shanghai, China. [3]Key Laboratory of RNA Science and Engineering, Shanghai Institute of Biochemistry and Cell Biology, Center for Excellence in Molecular Cell Science, Chinese Academy of Sciences, University of Chinese Academy of Sciences, Shanghai, China. [4]School of Life Science and Technology, ShanghaiTech University, Shanghai, China. [5]Center for Inflammatory Bowel Disease Research and Department of Gastroenterology, Shanghai Tenth People's Hospital, Tongji University School of Medicine, Shanghai, China. [6]Center for Infectious Disease Research, School of Medicine, Tsinghua University, Beijing, China. [7]Department of Immunology, Blavatnik Institute, Harvard Medical School, Boston, MA, USA. [8]These authors contributed equally: Tao Yang, Xiaohu Hu, Fei Cao. ✉e-mail: xinyang.song@sibcb.ac.cn; ycqian@sinh.ac.cn

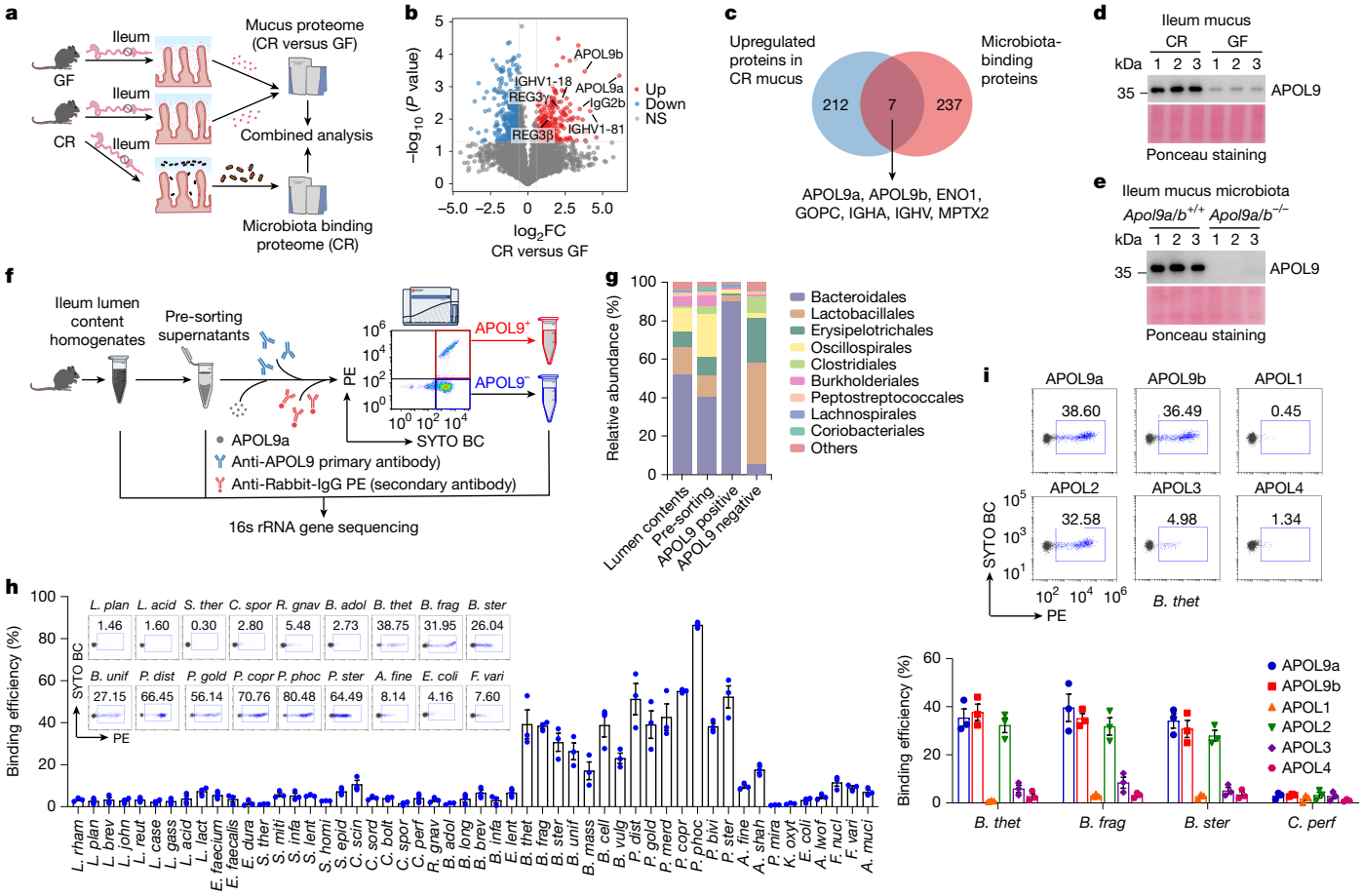

Fig. 1 | Identification of Bacteroidales as dominant APOL protein-binding symbionts. a, Schematic of proteomic analysis comparing ileal mucus proteins from conventionally raised (CR) and germ-free (GF) mice, alongside ileal microbiota-binding host proteins from CR mice. **b**, Proteins with increased levels in CR ($n = 3$) versus GF mice ($n = 3$) were identified by proteomic analysis. **c**, Venn diagram showing overlap candidates between upregulated mucus proteins in CR mice ($n = 3$) and microbiota-binding proteins. **d**,**e**, Immunoblot analysis of APOL9 levels in enriched ileal mucus proteins from wild-type (WT) CR and GF mice (**d**, $n = 3$) or total ileal microbiota lysates from *Apol9a*$^{+/+}$*Apol9b*$^{+/+}$ (*Apol9a/b*$^{+/+}$) and *Apol9a*$^{-/-}$*Apol9b*$^{-/-}$ (*Apol9a/b*$^{-/-}$) littermates (**e**, $n = 3$). **f**, Schematic diagram showing the flow sorting strategy of APOL9-bound ileal faecal bacteria for 16S rRNA gene sequencing. Samples from ileal lumen contents, purified ileal microbiota (pre-sorting supernatants) and APOL9-bound positive or negative ileal microbiota after flow cytometric sorting were analysed. **g**, The bacterial relative abundances at the order level are shown. **h**, Representative human commensal bacterial species from six phyla were individually incubated with recombinant mouse (rm) APOL9a, and the bacteria-APOL9a binding efficiencies were determined by flow cytometry. The representative flow cytometry plots are shown ($n = 3$). For full names and abbreviations of each bacterial strain, see Supplementary Table 3. **i**, Three representative *Bacteroides* species (*B. thetaiotaomicron*, *B. fragilis*, *Bacteroides stercoris*) and one *Clostridium* species (*Clostridium perfringens*) were individually incubated with rmAPOL9a and rmAPOL9b or recombinant human (rh) APOL1, APOL2, APOL3 and APOL4 protein. The binding efficiencies were determined by flow cytometry and the representative flow cytometry plots are shown ($n = 3$). Data are pooled from two or three independent experiments (**b**,**c**,**h**) or are representative of two (**g**,**i**) or three independent experiments (**d**,**e**). *n* represents biologically independent samples (**h**,**i**) or biologically independent animals (**b**–**e**). Data are presented as mean ± s.e.m. Statistical analysis was performed using one-way analysis of variance (ANOVA) followed by the false discovery rate (FDR) procedure (**b**). For gel source data, see Supplementary Fig. 2. FC, fold change; NS, not significant.

understand how the host's intestinal mucosal barrier responds to microbial stimuli, we first used label-free quantitative proteomics to identify host secretory factors whose levels in ileal mucus are altered in germ-free mice lacking microbiota (Fig. 1a). In parallel, the microbiota-binding host factors were also analysed through proteomics after enriching the microbial compartment from the ileal mucus of conventionally raised mice (specific pathogen-free (SPF)) (Fig. 1a). Using this strategy, we identified 219 proteins that are upregulated in the ileal mucosal layer of conventionally raised mice and 244 proteins that adhere to the ileal microbiota of these mice (Fig. 1b,c and Supplementary Tables 1 and 2). We also observed seven proteins that meet both criteria (Fig. 1c), including bacterial-coating IgA, whose level was induced by microbial colonization[24]. Notably, in addition to immunoglobulin molecules, we noticed that apolipoprotein L9a/b (APOL9a/b), two uncharacterized microbiota-binding proteins, are also enriched in the conventionally raised ileal mucus (Fig. 1b,c).

Apol9a/b belong to the APOL family and have been identified as interferon-stimulated genes[25,26]. However, they have not been associated with targeting commensal microorganisms. In mice, high expression levels of *Apol9a/b* were observed in both gut and liver tissues, with a particularly high abundance in various segments of the small intestine (Extended Data Fig. 1a). In the small intestine, *Apol9a/b* were selectively expressed in IECs rather than lymphoid compartments (Extended Data Fig. 1b). Consistent with our proteomics data (Fig. 1b), both transcripts of *Apol9a/b* were reduced in IECs from germ-free mice (Extended Data Fig. 1c). The APOL9 antibody can recognize both gene products as the coding sequences of both genes are almost identical. Thereby, a consistently decreased detection of APOL9 proteins was observed in germ-free or SPF mice treated with antibiotics (ABX) (Extended Data Fig. 1d,e). Furthermore, our findings indicated that the expression of *Apol9a/b* was compromised in both *Ifnar1*- and *Ifngr1*-deficient IECs, suggesting microbiota-dependent interferon signalling pathways

are involved in regulating ileal APOL9a/b production (Extended Data Fig. 1f–i). To further dissect their cellular sources and functions in the small intestine, we generated *Apol9a/b*-deficient mice using CRISPR–Cas9-mediated genome editing (Extended Data Fig. 2a). An insertion mutation was introduced into both gene loci, resulting in a loss of protein production for both genes in ileal IECs (Extended Data Fig. 2b–d). Unlike many AMPs that are produced by Paneth cells located at the bottom of intestinal crypts, we demonstrated that *Apol9a/b* were selectively expressed in enterocytes at the top of intestinal villi, as shown in a previously published single-cell RNA sequencing (scRNA-seq) study of IECs[27] (Extended Data Fig. 2e). The validation of this observation was further confirmed through immunofluorescence staining of ileal APOL9 in SPF wild-type, germ-free wild-type and *Apol9a/b*-deficient mice (Extended Data Fig. 2f).

Gut APOL9a/b target Bacteroidales

Next, we aimed to determine the functions of secreted APOL9. We validated a decrease in the level of ileal mucus APOL9 in Fig. 1b by immunoblotting with APOL9 antibody (Fig. 1d). A deficiency of *Apol9a/b* also blocked the deposition of APOL9 on microbiota located in the ileal mucus (Fig. 1e). To profile APOL9a/b microbial recognition, we purified recombinant APOL9a protein (Extended Data Fig. 3a) and developed a flow cytometry/16S taxonomy-based APOL9-seq strategy to evaluate the binding selectivity of APOL9a to a complex mouse gut microbiota (Fig. 1f). The recombinant APOL9a protein showed a remarkable preference for binding to mouse gut commensal bacteria from the Bacteroidales order (Fig. 1g). We also assessed the binding of APOL9a to 52 human gut microbial strains from six major bacterial phyla (Supplementary Table 3) by flow cytometry, and observed similar binding preference of APOL9a to human *Bacteroides*, *Parabacteroides*, *Prevotella* and *Alistipes* strains (Fig. 1h). Consistently, the recombinant APOL9b also bound to the same catalogue of human microbial strains (Fig. 1i and Extended Data Fig. 3b). To determine whether humans evolved a conserved microbial binding selectivity, we searched for the human equivalent of mouse APOL9 proteins and purified the corresponding recombinant proteins (Extended Data Fig. 3c–e). We found that human APOL1–APOL4 were structurally homologous to mouse APOL9a/b and were expressed in human enterocytes[28] (Extended Data Fig. 3c,d,f). We then sought to assess their microbial binding specificity by flow cytometry and we found that the recombinant human APOL2 could bind to Bacteroidales strains as efficiently as mouse APOL9a/b (Fig. 1i). These data suggest that both mouse and human gut APOL molecules bind to microorganisms in a conserved manner and have a preference for engaging Bacteroidales species within the gut microbiome.

Commensal Cer1Ps mediate the binding

To gain molecular insight into how APOL9a binds to commensal Bacteroidales, we selected *Bacteroides thetaiotaomicron* for the mechanistic studies, as this species dominates the human gut and is genetically tractable[29]. A previous study reported that APOL members can bind to eukaryotic anionic phospholipids[30]. One unique feature of Bacteroidetes is their ability to synthesize sphingolipids de novo using a serine-palmitoyltransferase (SPT) homologous to mammalian orthologues[31,32], leading us to speculate that the microbial sphingolipid biosynthesis and its products might be involved in APOL9a binding (Fig. 2a).

To test this hypothesis, we generated a series of gene knockout strains for the sphingolipid biosynthesis pathways in *B. thetaiotaomicron* (Fig. 2a). These included knockout strains for SPT (BT_0870 (refs. 31,32)), ceramide synthase (BT_3032, orthologue to ccna_01212 in *Caulobacter crescentus*[33]), ceramide kinase (BT_0871, orthologue to ccna_01218 in *C. crescentus*[34]), phosphoinositol dihydroceramide (PI-DHC) synthase (BT_1522 (ref. 35)) and myo-inositol phosphate (MIP) synthase (BT_1526 (ref. 35)). Loss of the getaway enzyme of sphingolipid biosynthesis, SPT or the subsequent ceramide synthase in *B. thetaiotaomicron* completely abolished the binding of APOL9a to the bacterium (Fig. 2b,c), indicating that downstream bacterial ceramide molecules are probably involved in mediating the APOL9 binding. More importantly, we elucidated that the ceramide kinase, but not PI-DHC and MIP synthase, was required for the bacterium to bind to APOL9a (Fig. 2b,c). Furthermore, we found that the ceramide kinase was also required for mouse APOL9b and human APOL2 to bind to *B. thetaiotaomicron* (Fig. 2d,e). A recent study has shown the presence of a bacterial ceramide kinase in *C. crescentus*[34], and we found that the *B. thetaiotaomicron* ceramide kinase orthologue was also responsible for the biosynthesis of microbial ceramide-1-phosphate (Cer1P) molecules (Fig. 2f and Supplementary Table 4). In addition, we investigated the presence of the Cer1P biosynthetic pathway in other Bacteroidales species used in our study, as well as datasets from the Human Microbiome Project[36]. From the phylogenetic analysis, we found that the Cer1P biosynthetic pathway genes (homologues to BT_0870, BT_3075, BT_3032 and BT_0871) were predominantly present in Bacteroidales (Extended Data Fig. 4a,b and Supplementary Table 5). However, the Cer1P biosynthetic pathway was less conserved in *Alistipes* species, which was consistent with their relatively weak binding to APOL9a in all the relevant Bacteroidales species we tested (Fig. 1h and Extended Data Fig. 4a,b). Thus, our findings suggest that both mouse and human APOL proteins are likely to bind to commensal Bacteroidales species through their membrane anionic Cer1Ps rather than other lipids.

We next sought to determine whether APOL proteins could bind directly to microbial Cer1P molecules. Using a lipid immunoprecipitation–mass spectrometry approach, we showed that recombinant APOL9a bound to *B. thetaiotaomicron* Cer1Ps with high affinity (Fig. 2g and Supplementary Table 6). To further test the direct binding between APOL proteins and *B. thetaiotaomicron* Cer1Ps, we obtained ceramide extracts from the bacterium by thin-layer chromatography (TLC) and performed a ceramide kinase reaction to generate Cer1Ps in vitro (Fig. 2h,i and Supplementary Table 7). We found that the recombinant ceramide kinase (BT_0871) converted *B. thetaiotaomicron* ceramides to their phosphorylated forms, whereas a kinase-dead protein failed to convert in the kinase assay (Fig. 2h,i and Extended Data Fig. 4c). Lastly, we found that both mouse APOL9a/b and human APOL2 strongly bound to re-extracted *B. thetaiotaomicron* Cer1Ps, but not to their ceramide precursors, using an in vitro protein–lipid overlay assay (Fig. 2j). Together, our data demonstrate that BT_0871 is a ceramide kinase for Cer1P biosynthesis in *B. thetaiotaomicron* and that host APOL proteins bind to this bacterium through a direct interaction with Cer1P molecules.

APOL9a/b induce OMV releasing

As members of the APOL family have been shown to have membrane pore-forming properties[37,38] and mediate the clearance of intracellular pathogens[39], we assessed the bactericidal activity of APOL9 deposition on *B. thetaiotaomicron*. Through immunofluorescence staining, it was observed that both APOL9a/b and APOL2 can deposit onto the membrane of *B. thetaiotaomicron* (Fig. 3a). To test whether APOL9 shows bactericidal activity in vivo in the gut, we investigated the microbiota compositions at different ileal loci by 16S ribosomal RNA gene sequencing (Fig. 3b–d). We observed comparable relative abundances and compositions of Bacteroidales and other bacteria in both the ileal luminal contents and mucus layers of wild-type and *Apol9a/b*-deficient mice (Fig. 3b–d). In addition, in vitro exposure to APOL9a or APOL9b did not interfere with the growth of *B. thetaiotaomicron* (Fig. 3e), although high doses of APOL9 proteins showed minor growth inhibitory effects on the strain (Extended Data Fig. 5a). We also found that adjusting culture parameters such as pH or NaCl concentration did not affect

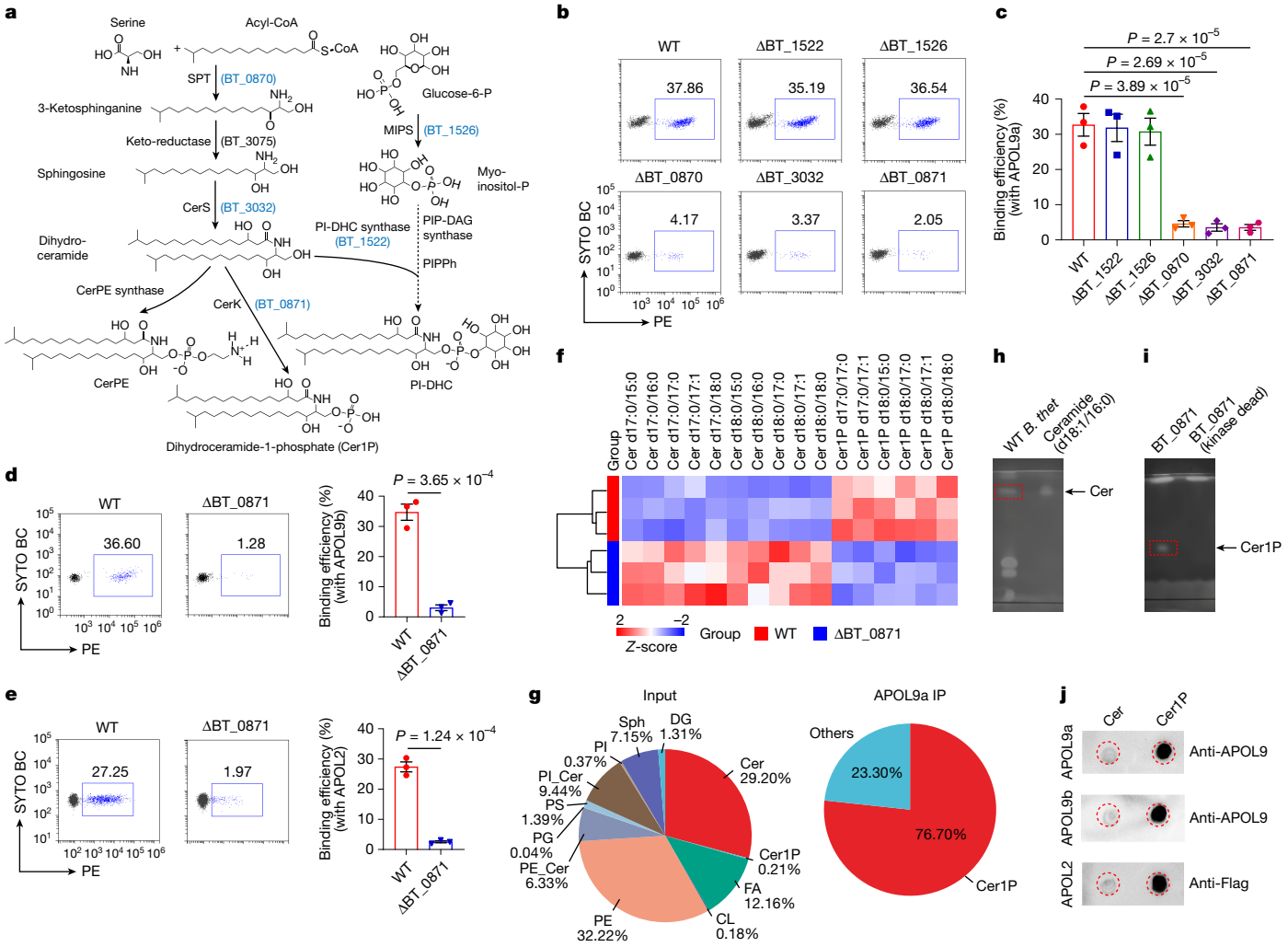

Fig. 2 | APOL proteins bind to gut commensal Bacteroidales through Cer1Ps. a, Schematic diagram of sphingolipid biosynthesis pathways in *B. thetaiotaomicron*. **b**,**c**, WT or different sphingolipid biosynthesis gene mutant strains of *B. thetaiotaomicron* were individually incubated with rmAPOL9a, followed by flow cytometric analysis. The representative flow cytometry plots (**b**) or binding efficiencies (**c**) ($n = 3$) are shown. **d**,**e**, WT or BT_0871 *B. thetaiotaomicron* were individually incubated with rmAPOL9b (**d**) or rhAPOL2 (**e**), followed by flow cytometric analysis. The representative flow cytometry plots or binding efficiencies ($n = 3$) are shown. **f**, Total lipids were extracted from WT or BT_0871 *B. thetaiotaomicron* and the levels of ceramides and Cer1Ps were determined by lipidomics analysis. The relative abundance of each indicated sphingolipid is shown in the heatmap ($n = 3$). **g**, Relative abundance of the represented lipid species in the total lipid composition of intact (input) or APOL9a-immunoprecipitated (IP) *B. thetaiotaomicron* lipid extracts by lipidomics analysis ($n = 2$). **h**,**i**, Ceramides from *B. thetaiotaomicron* were separated by TLC, visualized with primuline staining (**h**) and subjected to in vitro lipid kinase assays with recombinant CerK (BT_0871) or kinase-dead CerK as control (**i**). **j**, Lipid–protein overlay assays were then performed to evaluate the binding of APOL9a, APOL9b and APOL2 (Flag-tagged) to ceramides (Cer) or the resulting Cer1Ps. Data are representative of two (**f**–**j**) or three independent experiments (**b**–**e**). *n* represents biologically independent samples (**c**–**g**). Data are presented as mean ± s.e.m. Statistical analysis was performed using two-tailed Student's *t*-test (**d**,**e**) or one-way ANOVA followed by Bonferroni post hoc test (**c**). For gel source data, see Supplementary Fig. 2. CerS, ceramide synthase; CerK, ceramide kinase; MIPS, MIP synthase; PIP-DAG synthase, CDP-diacylglycerol-inositol 3-phosphatidyltransferase; PIPPh, phosphatidylinositol phosphate phosphatase.

the survival of *B. thetaiotaomicron* in the presence of either APOL9a or APOL9b (Extended Data Fig. 5b,c). Altogether, these data suggest that APOL9 may not have strong bactericidal activity against commensal bacteria under physiological conditions.

However, we observed a bacterial membrane bubbling phenomenon in APOL9a-incubated *B. thetaiotaomicron*, as shown by transmission electron microscopy (TEM) (Fig. 3f). Similar phenomena were also observed in other APOL9a-incubated Bacteroidales species such as *B. fragilis*, *Bacteroides vulgatus*, *Parabacteroides distasonis* and *Parabacteroides goldsteinii* (Extended Data Fig. 5d). This indicates that APOL9a deposition triggers membrane stress and subsequently enhances outer membrane vesicle (OMV) production in these bacteria. As APOL9a did not bind to *Escherichia coli* (Fig. 1h), its incubation did not induce OMV production in this species (Extended Data Fig. 5e). We also made consistent observations when APOL9b or APOL2 was incubated with Bacteroidales species or *E. coli* (Fig. 3f and Extended Data Fig. 5d,e). To quantify the OMV release upon incubation with mouse APOL9a/b or human APOL2, OMVs were collected from the *B. thetaiotaomicron* cultural supernatants and counted under TEM. The results showed that all three APOL proteins can promote OMV production in *B. thetaiotaomicron* (Fig. 3g,h). However, loss of Cer1P synthesis in the bacterium blocked excessive OMV production induced by APOL molecules (Fig. 3g,h). In addition, host APOL proteins also promoted OMV production from four other Bacteroidales species tested (Extended Data Fig. 5f), suggesting a conserved role for OMV release upon APOL protein deposition.

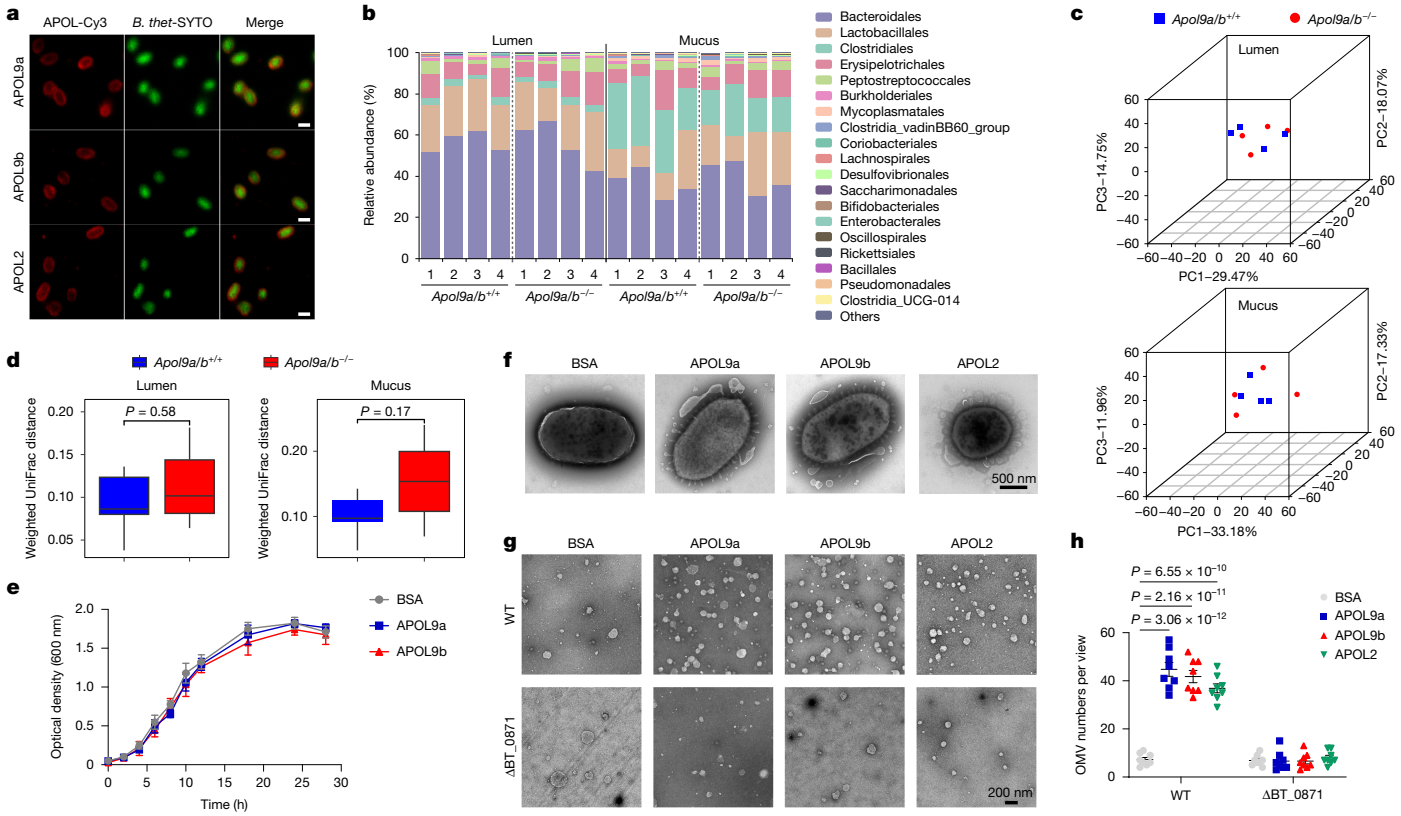

Fig. 3 | Targeting gut Bacteroidales by APOL proteins induces commensal OMV release. a, RmAPOL9a, rmAPOL9b or rhAPOL2 were conjugated with Cy3 (red), followed by incubation with SYTO BC pre-labelled *B. thetaiotaomicron*. The bacterial coatings by indicated APOL proteins were mounted under the microscope. Representative immunofluorescence images are shown. **b**–**d**, 16S rRNA gene sequencing of microbial compositions of the ileal lumen or mucus contents from *Apol9a/b*$^{+/+}$ ($n = 4$) and *Apol9a/b*$^{-/-}$ ($n = 4$) mice. Relative abundances (**b**), principal component analysis (PCA) plots (**c**) or weighted UniFrac distances (**d**) of bacterial orders are shown. **e**, Growth curves of *B. thetaiotaomicron* incubated with BSA, rmAPOL9a or rmAPOL9b under anaerobic conditions ($n = 3$). **f**, *B. thetaiotaomicron* was incubated with BSA, rmAPOL9a, rmAPOL9b or rhAPOL2 for 3 h under anaerobic conditions, followed by TEM observation. Representative images of single *B. thetaiotaomicron*-producing OMVs are shown. **g**,**h**, WT or BT_0871 *B. thetaiotaomicron* were individually incubated with BSA, rmAPOL9a, rmAPOL9b or rhAPOL2 for 6 h under anaerobic conditions. The OMVs produced in the bacterial culture supernatant were collected by ultracentrifuge and counted under TEM. The representative TEM images (**g**) or OMV numbers per view ($n = 8$) are shown (**h**). Data are representative of two (**a**,**e**) or three independent experiments (**b**–**d**,**f**–**h**). *n* represents biologically independent animals (**b**–**d**) or biological replicates (**e**,**h**). Data are presented as mean ± s.e.m. The box shows the respective 25th and 75th percentiles, the line within the box represents the median value and the whiskers show the lowest and highest data points still within 1.5 times the interquartile range of the respective lower and upper quartiles (**d**). Statistical analysis was performed using two-tailed Student's *t*-test (**d**,**e**) or one-way ANOVA followed by Bonferroni post hoc test (**h**). Scale bars, 1 μm (**a**), 500 nm (**f**), 200 nm (**g**). PC, principal component.

To investigate how host APOL proteins induce OMV release, we incubated mouse APOL9a or human APOL2 with either wild-type or Cer1P-deficient *B. thetaiotaomicron* and performed RNA sequencing (RNA-seq) on these bacteria. The transcriptomic data showed that both APOL9a and APOL2 exposure significantly induced genes involved in microbial cell membrane biogenesis and defence processes, including RpoE (BT_4647), OmpA family (BT_1194, BT_1391) and TolC family (BT_1267, BT_0954, BT_1695), in wild-type but not Cer1P-deficient *B. thetaiotaomicron* (Extended Data Fig. 5g–j). These findings show the microbial pathways involved in APOL protein-induced OMV production and lead us to further investigate whether APOL proteins can modulate host gut barrier functions through commensal OMVs.

OMVs promote IEC MHC-II expression

Symbiont-derived OMVs have demonstrated bioactivity under various immune contexts[40–42]. We first compared the size and composition of *B. thetaiotaomicron* OMVs released under steady-state or APOL9-incubated conditions. However, we did not observe significant differences in OMV size distribution, protein, DNA,/ RNA, lipopolysaccharide (LPS) or peptidoglycan cargo levels or membrane lipid composition between the groups (Extended Data Fig. 6a–c and Supplementary Table 8), suggesting that APOL9 deposition leads only to excess OMV production but does not affect its composition.

Next, we performed a transcriptome profiling of ileal IECs and found that APOL9 deficiency led to a downregulation of epithelial major histocompatibility complex class II (MHC-II) molecules in these mice (Fig. 4a). The RNA-seq results were also validated by PCR with reverse transcription and flow cytometry quantification on ileal epithelial MHC-II levels of both wild-type and *Apol9a/b*-deficient mice (Fig. 4b,c). To test whether commensal-derived OMVs may modulate immune pathways in intraepithelial cells that are involved in MHC-II induction in IECs, we applied a dendritic cell (DC)–IEL–IEC Transwell co-culture system incubated with OMV stimulus (Fig. 4d). We found that OMVs derived from *B. thetaiotaomicron* significantly increased the production of interferon-γ (IFNγ), a key cytokine for inducing MHC-II in the gut epithelium[43], in the DC–IEL co-culture scenario (Fig. 4e). Consistently, we found that incubating OMVs with DCs and IELs in the Transwell insert significantly enhanced the expression of MHC-II molecules in basolateral co-cultured IECs (Fig. 4f). In addition, we

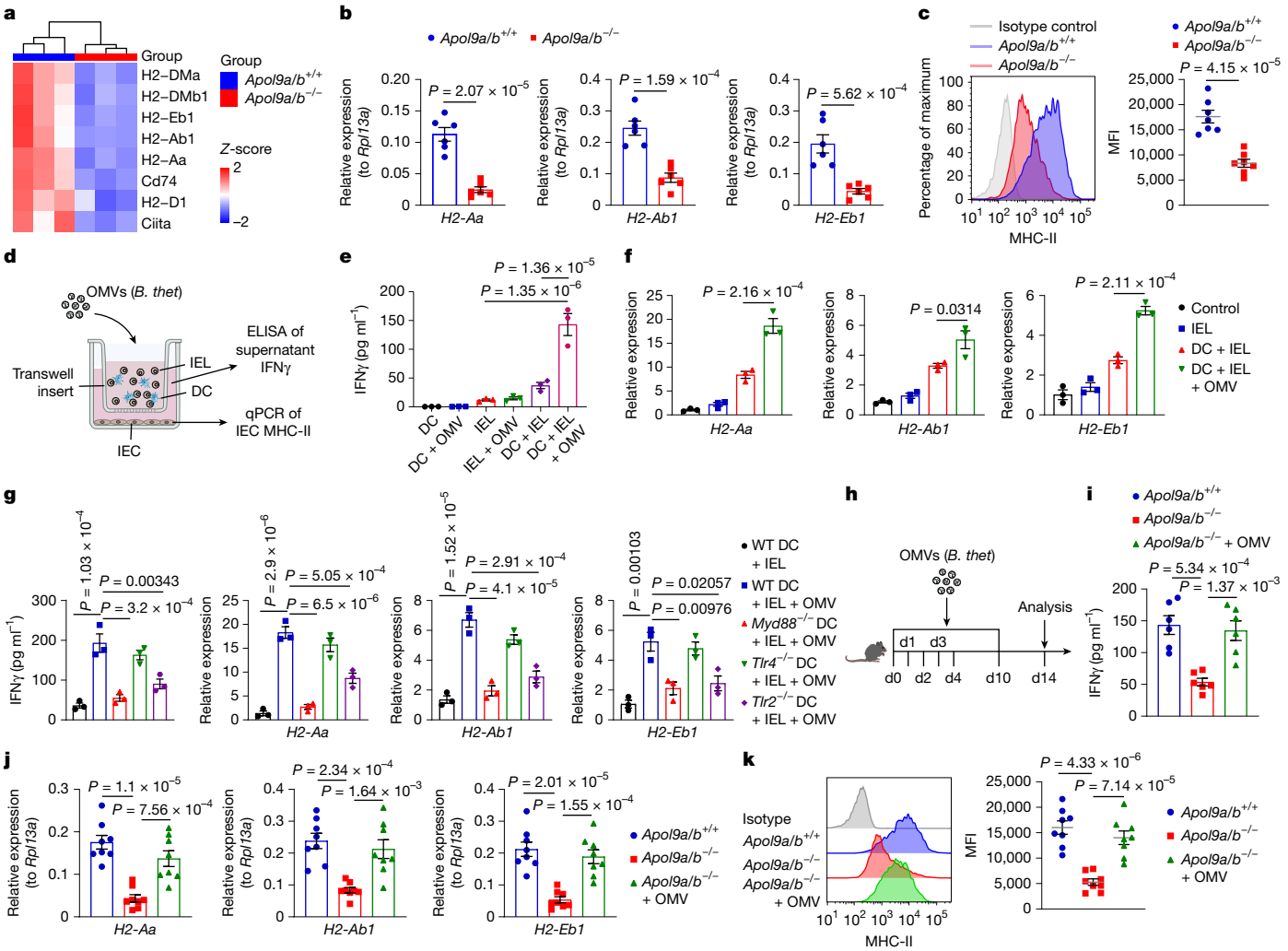

Fig. 4 | Bacteroidales-derived OMVs promote MHC-II gene expression in ileal ECs. a, Bulk RNA-seq analysis of ileal epithelial cell (ECs) from *Apol9a/b*$^{+/+}$ ($n = 3$) and *Apol9a/b*$^{-/-}$ ($n = 3$) mice. Heatmap showing the downregulation of MHC-II genes in ileal ECs from *Apol9a/b*$^{-/-}$ mice compared with *Apol9a/b*$^{+/+}$ mice. **b**,**c**, Quantitative PCR (qPCR) (**b**, $n = 6$) and flow cytometry (**c**, $n = 7$) validation of the downregulation of representative MHC-II genes in ileal ECs from *Apol9a/b*$^{-/-}$ mice. **d**, Schematic of co-cultures of primary ileal ECs with IEL–DC contacts under *B. thetaiotaomicron*-derived OMV incubation in a Transwell system. **e**,**f**, ELISA analysis of supernatant IFNγ production (**e**, $n = 3$) and qPCR analysis of MHC-II gene expression (**f**, $n = 3$) in ileal ECs are shown. **g**, ELISA analysis of supernatant IFNγ production (left) or qPCR analysis of MHC-II gene expression in ileal ECs (right) in a Transwell co-culture of WT, *Myd88*$^{-/-}$, *Tlr4*$^{-/-}$ or *Tlr2*$^{-/-}$ DCs with IELs under *B. thetaiotaomicron*-derived OMV incubation ($n = 3$). **h**, Schematic diagram of *Apol9a/b*$^{-/-}$ mice administered orally with OMVs derived from *B. thetaiotaomicron*. Tissues or cells were analysed on day 14. **i**, ELISA analysis of ileal IFNγ production from *Apol9a/b*$^{+/+}$, *Apol9a/b*$^{-/-}$ and *Apol9a/b*$^{-/-}$ mice administered with OMVs ($n = 6$). **j**,**k**, qPCR (**j**) and flow cytometry (**k**) analysis of representative MHC-II molecule expression in ileal ECs from *Apol9a/b*$^{+/+}$, *Apol9a/b*$^{-/-}$ and *Apol9a/b*$^{-/-}$ mice administered with OMVs ($n = 8$). Data are pooled from two independent experiments (**a**,**i**,**j**) or are representative of two (**g**,**k**) or three independent experiments (**b**,**c**,**e**,**f**). *n* represents biologically independent samples (**e**–**g**) or biologically independent animals (**a**–**c**,**i**–**k**). Data are presented as mean ± s.e.m. Statistical analysis was performed using two-tailed Student's *t*-test (**b**,**c**) or one-way ANOVA followed by Bonferroni post hoc test (**e**–**g**,**i**–**k**). MFI, mean fluorescence intensity.

showed OMVs derived from both steady-state and APOL9 incubation induced similar levels of IFNγ production and MCH-II expression in the co-culture system (Extended Data Fig. 6d,e). As bacterial OMVs are sensed by innate pathways in DCs[40–42], we also demonstrated that *B. thetaiotaomicron*-derived OMVs stimulate gut IFNγ and MHC-II in a TLR2-MyD88 signalling-dependent manner, whereas the TLR4 signalling was less necessary under the setting (Fig. 4g).

To examine whether the loss of MHC-II expression in *Apol9a/b*-deficient ileal epithelial cells was caused by a reduced level of microbial OMVs, we orally treated *Apol9a/b*-deficient mice with *B. thetaiotaomicron*-derived OMVs (Fig. 4h). Consistent with our in vitro observation, in vivo administration of OMVs rescued ileal IFNγ levels comparable to wild-type counterparts (Fig. 4i) and consequently restored the expression of epithelial MHC-II molecules in *Apol9a/b*-deficient ilea (Fig. 4j,k). Thus, our results suggest that APOL9 can induce the release of *Bacteroides* OMVs, which promotes epithelial MHC-II expression through multicellular interactions.

APOL9a/b modulate gut IELs and infection

As epithelial MHC-II molecules have a crucial role in maintaining immunological homeostasis in the gut[43], we conducted an scRNA-seq survey of CD45^{+} immune cells from the ileal intraepithelial region of both wild-type and *Apol9a/b*-deficient mice (Fig. 5a and Extended Data Fig. 7a,b). The deletion of *Apol9a/b* in mice did not affect the general composition of intraepithelial immune cells (Fig. 5a). However, we observed a significant reduction in ileal CD4^{+}CD8αα^{+} IELs as well as lymphocyte signature gene expression in these IELs upon

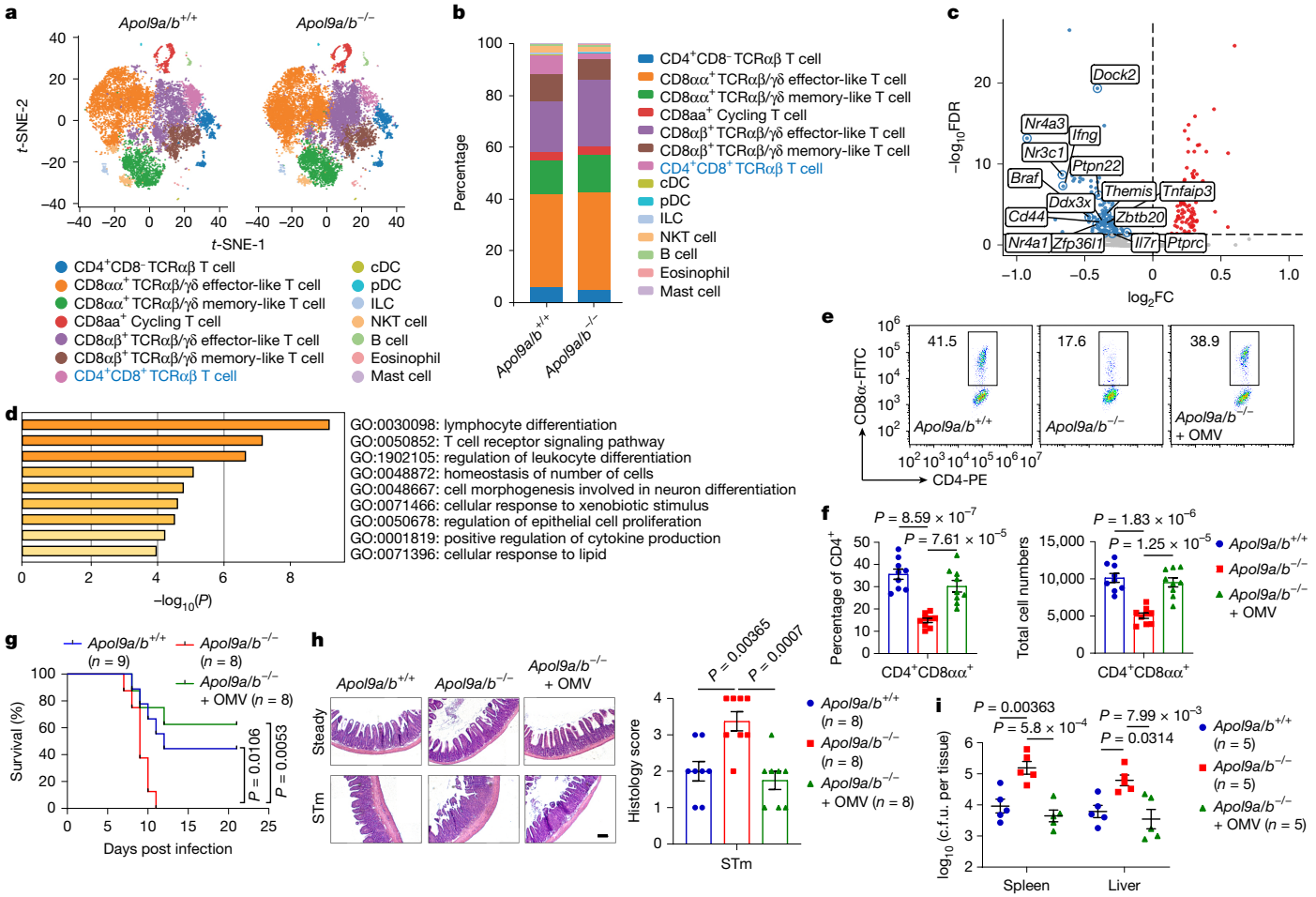

Fig. 5 | APOL9a/b control intraepithelial CD4$^+$CD8αα$^+$ cells and mucosal infection. a–**d**, scRNA-seq of flow cytometry-sorted ileal intraepithelial CD45$^+$ immune cells pooled from *Apol9a/b*$^{+/+}$ ($n = 7$) or *Apol9a/b*$^{-/-}$ ($n = 6$) mice. **a**, *t*-distributed stochastic neighbour embedding (*t*-SNE) plots of intraepithelial immune cells from *Apol9a/b*$^{+/+}$ or *Apol9a/b*$^{-/-}$ mice are shown. Individual points correspond to single cells. **b**, Histogram showing the proportion of intraepithelial CD45$^+$ immune cells between groups. **c**,**d**, Volcano plot (**c**) and Gene Ontology (**d**) analysis of the downregulated genes in CD4$^+$CD8αα$^+$ IELs from *Apol9a/b*$^{-/-}$ mice versus *Apol9a/b*$^{+/+}$ mice are shown. **e**,**f**, Flow cytometry analysis of ileal CD4$^+$CD8αα$^+$ IELs from *Apol9a/b*$^{+/+}$, *Apol9a/b*$^{-/-}$ and *Apol9a/b*$^{-/-}$ mice administered with OMVs. The representative flow cytometry plots (**e**), CD4$^+$CD8αα$^+$ cell percentages and cell numbers (**f**) are shown ($n = 9$). **g**–**i**, STm infection of *Apol9a/b*$^{+/+}$, *Apol9a/b*$^{-/-}$ and *Apol9a/b*$^{-/-}$ mice administered with OMVs. Survival curves (**g**, $n = 9$ or 8), ileal histology (day 5) (**h**, $n = 8$) and bacterial quantification (day 5) in the spleen and liver (**i**, $n = 5$) are shown. Data are pooled from two independent experiments (**a**–**d**) or are representative of three independent experiments (**e**–**i**). *n* represents biologically independent animals (**a**–**i**). Data are presented as mean ± s.e.m. Statistical analysis was performed using a Wilcoxon test (**c**), one-way ANOVA followed by Bonferroni post hoc test (**f**,**h**,**i**) or log-rank (Mantel–Cox) test (**g**). Scale bar, 10 µm. c.f.u., colony-forming units; cDC, conventional dendritic cells; pDC, plasmacytoid dendritic cells; ILC, innate lymphoid cells; NKT cell, natural killer T cells.

Apol9a/b deficiency (Fig. 5a–d and Extended Data Fig. 7c). Using flow cytometry, we confirmed that the deficiency of *Apol9a/b* resulted in a reduced level of ileal CD4$^+$CD8αα$^+$ IELs, whereas the proportions of other IEL or lamina propria lymphocyte (LPL) compartments remained unaffected (Fig. 5e,f and Extended Data Fig. 7d,e). We also observed that the decrease of CD4$^+$CD8αα$^+$ IELs occurred mainly in the ileum, with no change in the duodenum and a modest decrease in the jejunum (Extended Data Fig. 7f). In addition, we found that OMV administration in *Apol9a/b*-deficient mice not only restored epithelial MHC-II levels but also rescued CD4$^+$CD8αα$^+$ IEL levels in these mice (Figs. 4j,k and 5e,f). This observation is consistent with a previous study that found a decrease in ileal CD4$^+$CD8αα$^+$ IEL levels owing to loss of epithelial MHC-II (ref. 44).

To further investigate the in vivo APOL9–*Bacteroides* interaction and its impact on ileal intraepithelial immunity, we first used a broad-spectrum combination of ABX to deplete the endogenous microbiota of either *Apol9a/b*-deficient mice or their wild-type littermates, and then reconstituted their microbiota by faecal material transfer (FMT) of a mouse microbiota largely devoid of Bacteroidales species (Extended Data Fig. 8a,b). We found that ABX treatment significantly impaired the levels of ileal epithelial MHC-II molecules and CD4$^+$CD8αα$^+$ IELs, whereas reconstitution of Bacteroidales-lacking microbiota restored these intraepithelial immune parameters to comparable levels between the groups, although the levels were compromised compared with mice normally harbouring Bacteroidales in our facility (Figs. 4i–k and 5e,f and Extended Data Fig. 8c–g). These data suggest that the immunomodulatory function of APOL9 in vivo is likely to be Bacteroidales-dependent.

We next sought to determine whether APOL9 proteins modulate ileal intraepithelial immunity in vivo through *Bacteroides*-deposition. To test this, we reconstituted the microbiota of ABX-treated *Apol9a/b*-deficient mice and their wild-type littermates with FMT of Bacteroidales-lacking microbiota plus either wild-type or BT_0871-deficient *B. thetaiotaomicron* strain. We found that both *B. thetaiotaomicron* strains colonized the intestines of both *Apol9a/b*-deficient mice and their wild-type littermates to a comparable extent (Extended Data Fig. 9a).

However, only reconstitution of the wild-type *B. thetaiotaomicron* strain in *Apol9a/b*-sufficient mice elicited higher levels of ileal IFNγ, MHC-II and $CD4^+CD8\alpha\alpha^+$ IELs, whereas neither the wild-type *B. thetaiotaomicron* strain reconstituted in *Apol9a/b*-deficient mice nor the BT_0871-deficient *B. thetaiotaomicron* strain reconstituted in *Apol9a/b*-sufficient or -deficient mice could further induce these intraepithelial immune parameters (Extended Data Fig. 9b–f). Thus, consistent with our in vitro observations, these results suggest that the in vivo effect of APOL9 proteins on ileal intraepithelial immunity is also dependent on their binding to *Bacteroides* and the subsequent release of OMVs.

Ileal $CD4^+CD8\alpha\alpha^+$ IELs have been shown to possess both cytotoxic and regulatory properties, and are crucial for maintaining immune tolerance and anti-infection responses in the gut[10,45]. Therefore, we examined whether APOL9a/b affect gut defence responses in a *Salmonella typhimurium* (STm) oral infection model. Our findings indicated that APOL9a/b neither directly bound to and killed STm nor were required for the intracellular clearance of the organism (Extended Data Fig. 10a–d). However, mice deficient in *Apol9a/b* exhibited higher mortality rates (Fig. 5g), more severe gut inflammation (Fig. 5h), and greater gut bacterial burden and dissemination to non-gut organs (Fig. 5i and Extended Data Fig. 10e), whereas OMV administration ameliorated STm infection in *Apol9a/b*-deficient mice (Fig. 5g–i). Furthermore, we did not observe a protective role of APOL9 against STm oral infection in the Bacteroidales-lacking microbiota reconstituted mice (Extended Data Fig. 10f–h), or against STm systemic infection (Extended Data Fig. 10i,j). Together, these results suggest that APOL9a and APOL9b have a protective role during enteric infection through their immunomodulatory function in the gut.

Discussion

Proper intestinal–microbial mutualism is critical to maintaining organ homeostasis. To prevent tissue perturbations caused by gut microorganisms, the host develops strategies to target microbiota for immunological defence. For example, specialized intestinal cells secrete AMPs[14], immunoglobulins[20–22] and complements[15] to remove harmful microorganisms and restrict the symbiotes to the intestinal lumen. In response, gut commensal bacteria evolve adaptation tactics to maintain their stability in the mammalian gut for extended periods. A previous study demonstrated that members of the Bacteroidetes phylum develop resistance to AMPs by dephosphorylating their LPSs, which allows them to thrive in the host gut[46]. Our study delineates a new mechanism for tackling mutual coexistence in the scenario of host–Bacteroidales interactions.

Unlike other known bacterial-coating proteins, we have identified that mouse APOL9a/b and their human equivalent APOL2 preferentially target commensal Bacteroidales species. Although many AMPs are secreted by intestinal Paneth cells or goblet cells, these APOL proteins are predominantly produced by enterocytes. Despite that they could weakly affect the in vitro survival of *B. thetaiotaomicron*, deficiency of *Apol9a/b* in mice does not disturb the overall composition of the gut microbiota, indicating that they do not exhibit strong bactericidal activity under static conditions. Instead, APOL9a/b bind to specific bacterial ceramide molecules to trigger bacterial membrane defence and biogenesis, leading to subsequent OMV production in *B. thetaiotaomicron*.

Bacterial OMVs have been shown to have immunomodulatory functions in several biological contexts[40–42], whereas our data show that both mouse and human APOL proteins can induce excessive OMV production in different *Bacteroides* species, suggesting a conserved host-modulating role of this phenomenon. We extend the current understanding of OMV biology by showing that these *Bacteroides*-derived OMVs can activate innate signalling in DCs, thereby promoting IFNγ production in IELs and subsequent MHC-II expression in ileal epithelial cells. This multicellular communication gives rise to a distinct population of ileal $CD4^+$ IELs expressing CD8αα, which mediate mucosal immunity against infection with enteric pathogens; however, future work is needed to understand how these $CD4^+CD8\alpha\alpha^+$ IELs control enteric infection. In summary, our study demonstrates that *Bacteroides*-derived OMVs can improve gut barrier function by mediating IEC–immune crosstalk at the mucosal interface. These findings also improve our understanding of how hosts benefit from mutualistic relationships with commensal bacteria through the microbiota-targeting proteins they deploy.

Online content

Any methods, additional references, Nature Portfolio reporting summaries, source data, extended data, supplementary information, acknowledgements, peer review information; details of author contributions and competing interests; and statements of data and code availability are available at https://doi.org/10.1038/s41586-025-08990-4.

1. Donia, M. S. & Fischbach, M. A. Small molecules from the human microbiota. *Science* **349**, 1254766 (2015).
2. Krautkramer, K. A., Fan, J. & Backhed, F. Gut microbial metabolites as multi-kingdom intermediates. *Nat. Rev. Microbiol.* **19**, 77–94 (2021).
3. Arpaia, N. et al. Metabolites produced by commensal bacteria promote peripheral regulatory T-cell generation. *Nature* **504**, 451–455 (2013).
4. Smith, P. M. et al. The microbial metabolites, short-chain fatty acids, regulate colonic T_{reg} cell homeostasis. *Science* **341**, 569–573 (2013).
5. Furusawa, Y. et al. Commensal microbe-derived butyrate induces the differentiation of colonic regulatory T cells. *Nature* **504**, 446–450 (2013).
6. Hang, S. et al. Bile acid metabolites control T_H17 and T_{reg} cell differentiation. *Nature* **576**, 143–148 (2019).
7. Song, X. et al. Microbial bile acid metabolites modulate gut $ROR\gamma^+$ regulatory T cell homeostasis. *Nature* **577**, 410–415 (2020).
8. Campbell, C. et al. Bacterial metabolism of bile acids promotes generation of peripheral regulatory T cells. *Nature* **581**, 475–479 (2020).
9. Cervantes-Barragan, L. et al. *Lactobacillus reuteri* induces gut intraepithelial $CD4^+CD8\alpha\alpha^+$ T cells. *Science* **357**, 806–810 (2017).
10. Song, X. et al. Gut microbial fatty acid isomerization modulates intraepithelial T cells. *Nature* **619**, 837–843 (2023).
11. Mazmanian, S. K., Round, J. L. & Kasper, D. L. A microbial symbiosis factor prevents intestinal inflammatory disease. *Nature* **453**, 620–625 (2008).
12. Oh, S. F. et al. Host immunomodulatory lipids created by symbionts from dietary amino acids. *Nature* **600**, 302–307 (2021).
13. Peterson, L. W. & Artis, D. Intestinal epithelial cells: regulators of barrier function and immune homeostasis. *Nat. Rev. Immunol.* **14**, 141–153 (2014).
14. Mukherjee, S. & Hooper, L. V. Antimicrobial defense of the intestine. *Immunity* **42**, 28–39 (2015).
15. Wu, M. et al. Gut complement induced by the microbiota combats pathogens and spares commensals. *Cell* https://doi.org/10.1016/j.cell.2023.12.036 (2024).
16. Cash, H. L., Whitham, C. V., Behrendt, C. L. & Hooper, L. V. Symbiotic bacteria direct expression of an intestinal bactericidal lectin. *Science* **313**, 1126–1130 (2006).
17. Vaishnava, S. et al. The antibacterial lectin RegIIIγ promotes the spatial segregation of microbiota and host in the intestine. *Science* **334**, 255–258 (2011).
18. Bergstrom, J. H. et al. Gram-positive bacteria are held at a distance in the colon mucus by the lectin-like protein ZG16. *Proc. Natl Acad. Sci. USA* **113**, 13833–13838 (2016).
19. McPherson, R. L. et al. Lectin-Seq: a method to profile lectin-microbe interactions in native communities. *Sci. Adv.* **9**, eadd8766 (2023).
20. Palm, N. W. et al. Immunoglobulin A coating identifies colitogenic bacteria in inflammatory bowel disease. *Cell* **158**, 1000–1010 (2014).
21. Kau, A. L. et al. Functional characterization of IgA-targeted bacterial taxa from undernourished Malawian children that produce diet-dependent enteropathy. *Sci. Transl. Med.* **7**, 276ra224 (2015).
22. Shapiro, J. M. et al. Immunoglobulin A targets a unique subset of the microbiota in inflammatory bowel disease. *Cell Host Microbe* **29**, 83–93 e83 (2021).
23. Hooper, L. V. et al. Molecular analysis of commensal host-microbial relationships in the intestine. *Science* **291**, 881–884 (2001).
24. Geva-Zatorsky, N. et al. Mining the human gut microbiota for immunomodulatory organisms. *Cell* **168**, 928–943 e911 (2017).
25. Sun, L. et al. Type I interferons link viral infection to enhanced epithelial turnover and repair. *Cell Host Microbe* **17**, 85–97 (2015).
26. Kreit, M., Vertommen, D., Gillet, L. & Michiels, T. The interferon-inducible mouse apolipoprotein L9 and prohibitins cooperate to restrict Theiler's virus replication. *PLoS ONE* **10**, e0133190 (2015).
27. Haber, A. L. et al. A single-cell survey of the small intestinal epithelium. *Nature* **551**, 333–339 (2017).
28. Wang, Y. et al. Single-cell transcriptome analysis reveals differential nutrient absorption functions in human intestine. *J. Exp. Med.* https://doi.org/10.1084/jem.20191130 (2020).
29. Wexler, A. G. & Goodman, A. L. An insider's perspective: *Bacteroides* as a window into the microbiome. *Nat. Microbiol.* **2**, 17026 (2017).

30. Uzureau, S. et al. APOL1 C-terminal variants may trigger kidney disease through interference with APOL3 control of actomyosin. *Cell Rep.* **30**, 3821–3836 e3813 (2020).
31. Brown, E. M. et al. *Bacteroides*-derived sphingolipids are critical for maintaining intestinal homeostasis and symbiosis. *Cell Host Microbe* **25**, 668–680 e667 (2019).
32. Johnson, E. L. et al. Sphingolipids produced by gut bacteria enter host metabolic pathways impacting ceramide levels. *Nat. Commun.* **11**, 2471 (2020).
33. Stankeviciute, G. et al. Convergent evolution of bacterial ceramide synthesis. *Nat. Chem. Biol.* **18**, 305–312 (2022).
34. Dhakephalkar, T., Stukey, G. J., Guan, Z., Carman, G. M. & Klein, E. A. Characterization of an evolutionarily distinct bacterial ceramide kinase from *Caulobacter crescentus*. *J. Biol. Chem.* **299**, 104894 (2023).
35. Heaver, S. L. et al. Characterization of inositol lipid metabolism in gut-associated Bacteroidetes. *Nat. Microbiol.* **7**, 986–1000 (2022).
36. Lloyd-Price, J. et al. Multi-omics of the gut microbial ecosystem in inflammatory bowel diseases. *Nature* **569**, 655–662 (2019).
37. Perez-Morga, D. et al. Apolipoprotein L-I promotes trypanosome lysis by forming pores in lysosomal membranes. *Science* **309**, 469–472 (2005).
38. Thomson, R. & Finkelstein, A. Human trypanolytic factor APOL1 forms pH-gated cation-selective channels in planar lipid bilayers: relevance to trypanosome lysis. *Proc. Natl Acad. Sci. USA* **112**, 2894–2899 (2015).
39. Gaudet, R. G. et al. A human apolipoprotein L with detergent-like activity kills intracellular pathogens. *Science* https://doi.org/10.1126/science.abf8113 (2021).
40. Stefan, K. L., Kim, M. V., Iwasaki, A. & Kasper, D. L. Commensal microbiota modulation of natural resistance to virus infection. *Cell* **183**, 1312–1324 e1310 (2020).
41. Yang, D. et al. Dysregulated lung commensal bacteria drive interleukin-17B production to promote pulmonary fibrosis through their outer membrane vesicles. *Immunity* **50**, 692–706 e697 (2019).
42. Shen, Y. et al. Outer membrane vesicles of a human commensal mediate immune regulation and disease protection. *Cell Host Microbe* **12**, 509–520 (2012).
43. Heuberger, C., Pott, J. & Maloy, K. J. Why do intestinal epithelial cells express MHC class II? *Immunology* **162**, 357–367 (2021).
44. Moon, S. et al. Niche-specific MHC II and PD-L1 regulate $CD4^+CD8\alpha\alpha^+$ intraepithelial lymphocyte differentiation. *J. Exp. Med.* https://doi.org/10.1084/jem.20201665 (2021).
45. Lockhart, A., Mucida, D. & Bilate, A. M. Intraepithelial lymphocytes of the intestine. *Annu. Rev. Immunol.* https://doi.org/10.1146/annurev-immunol-090222-100246 (2024).
46. Cullen, T. W. et al. Antimicrobial peptide resistance mediates resilience of prominent gut commensals during inflammation. *Science* **347**, 170–175 (2015).

Methods

Mice

C57BL/6J mice maintained under SPF or germ-free conditions were purchased from Shanghai SLAC Laboratory Animal or Cyagen Biosciences. *Apol9a*$^{-/-}$*Apol9b*$^{-/-}$ (*Apol9a/b*$^{-/-}$) double-deficient mice were generated by CRISPR–Cas9 by the Shanghai Model Organisms Center. *Ifnar1*$^{-/-}$ and *Ifngr1*$^{-/-}$ mice were obtained from wild-type mice intercrossed with *Ifnar1*$^{-/-}$*Ifngr1*$^{-/-}$ double-deficient mice which were provided by Q. Leng. *Myd88*$^{-/-}$ mice were obtained from the Model Animal Research Center of Nanjing University (Nanjing, China). *Tlr2*$^{-/-}$ mice were purchased from Cyagen Biosciences. *Tlr4*$^{-/-}$ mice were provided by S. Zhu. A C57BL/6J mouse strain largely devoid of gut Bacteroidales was purchased from Shanghai LINGCHANG Biotech. All genetically modified mice and their control mice on the C57BL/6J background were subjected to experiments at the age of 6–12 weeks. Both male and female mice were used in this study. All animals were maintained under a 12-h/12-h light/dark cycle and received gamma-irradiated (50 kGy) pellet chow. A temperature of 20–24 °C and a humidity of 40–60% were used as housing conditions. All animal studies were conducted under the Guide for the Care and Use of Laboratory Animals and were approved by the Institutional Biomedical Research Ethics Committee of the Shanghai Institute of Nutrition and Health (SINH-2023-QYC-1), the Institutional Animal Care and Use Committee of the Center for Excellence in Molecular Cell Science (SIBCB-S748-2108-031, SIBCB-S748-2308-30) or the Shanghai Institute of Immunity and Infection (A2023018), Chinese Academy of Sciences.

Antibodies and recombinant cytokines

Rabbit polyclonal anti-GAPDH (AP0063, 1:2,000) was obtained from Bioworld. Rabbit polyclonal anti-transferrin (17435-1-AP, 1:500) was obtained from Proteintech. Rabbit monoclonal anti-His tag (12698, 1:500) and rabbit monoclonal anti-Flag tag (14793, 1:500) were obtained from CST. Anti-mouse APOL9 antibody (1:1,000) was raised in rabbits (Shanghai Ango Biological Technology) immunized with purified His-tagged APOL9a protein. Recombinant mouse IL-15 (566302) and mouse IL-3 (575502) were obtained from BioLegend. Recombinant mouse IL-2 (212-12), mouse IL-7 (217-17) and mouse EGF (315-09) were from Peprotech. Transferrin (T8158) was obtained from Sigma.

Bacterial strains and growth conditions

Anaerobic bacteria were grown on *Brucella* agar plates (Oxoid) supplemented with 5% sheep blood, 5 mg l^{-1} hemin and 2.5 mg l^{-1} vitamin K1, and then subcultured in Brain Heart Infusion Medium (Oxoid) supplemented with 5 mg l^{-1} hemin and 2.5 mg l^{-1} vitamin K1 (BHIS). *Lactobacillus* strains were cultured on MRS agar plates or in MRS broth (BD Difco). All bacteria were then cultured under anaerobic conditions (80% N_2, 10% H_2 and 10% CO_2) at 37 °C in an anaerobic chamber. The bacterial strains used are listed in Supplementary Table 3.

Genetical manipulation of bacteria

Deletion mutants were created in the *B. thetaiotaomicron* VPI-5482 background and constructed using previously described counter-selectable allele exchange methods[47]. In brief, approximately 1-kb fragments corresponding to the upstream and downstream regions of the target genes were PCR amplified and then fused by fusion PCR to generate approximately 2-kb products using the following primers: BT_0870 up forward: 5′-GTAAGATTAGCATTATGAGTGGATCCCCCTCGAATACACAACTTC-3′; BT_0870 up reverse: 5′-AGCTTTTCAGAGATGCTGCGAATTATAATTTATTATACTC-3′; BT_0870 down forward: 5′-GCAGCATCTCTGAAAAGCTAT-3′; BT_0870 down reverse: 5′-GAAGATAGGCAATTAGTCGACGGTATAATTATATATGTATCATT-3′; BT_0871 up forward: 5′-GTGTAAGATTAGCATTATGAGTGGATCCAGAAGAATCAGCAGCGATAA-3′; BT_0871 up reverse: 5′-ACAATAAATCAGAAATCGGCATTTATTTCTTTCGTTCATGCTAATCTT-3′; BT_0871 down forward: 5′-AATAAATGCCGATTTCTGATTTATTGTG-3′; BT_0871 down reverse: 5′-TGGAAGATAGGCAATTAGTCGACCAGAGAAACCATGACCTTTCAT-3′; BT_1522 up forward: 5′-GTGTAAGATTAGCATTATGAGTGGATCCAAACGCATGTTGCTGTAAAATT-3′; BT_1522 up reverse: 5′-ATA TATTGCGGTATTTGTTCTTCATTGAATTGTTTTTATCATTAAG-3′; BT_1522 down forward: 5′-TCAATGAAGAACAAATACCGCAATATATTC-3′; BT_1522 down reverse: 5′-CTGGAAGATAGGCAATTAGTCGACATAGTAAAATAAGGCTACTTTTTATT-3′; BT_1526 up forward: 5′-TAAGATTAGCATTATGAGTGGATCCCACAAGCAAAGACAATGTCTTCCTT-3′; BT_1526 up reverse: 5′-AACTTTCAACTCTCCACTTATTTAATTCTATTCTATTAAAATTAAACT-3′; BT_1526 down forward: 5′-AATTAAATAAGTGGAGAGTTGAAAGTTGA-3′; BT_1526 down reverse: 5′-ACTGGAAGATAGGCAATTAGTCGACGATGATGAAGAAGTCACCGA-3′; BT_3032 up forward: 5′-GGTGTAAGATTAGCATTATGAGTGGATCCTGTATCTTCACAAGGAATTGT-3′; BT_3032 up reverse: 5′-CAATTCGTTCTCTTCCATAGCTGATCTCGTATTTATGATTGAG-3′; BT_3032 down forward: 5′-AGATCAGCTATGGAAGAGAACGAATTGA-3′; BT_3032 down reverse: 5′-GATAGGCAATTAGTCGACGGAGTCATGTTGGTAGATCCCAGT-3′. The approximately 2-kb PCR products were cloned into the fragment of the pLGB13 vector using the Hieff Clone Plus One Step Cloning Kit (YEASEN). The resulting plasmids were transformed into *E. coli* S17-1 λ pir and then conjugated into *B. thetaiotaomicron* VPI-5482. The single crossover integrated Bacteroides strains were selected on BHIS plates containing 200 μg ml^{-1} gentamicin and 15 μg ml^{-1} erythromycin and plated on BHIS plates supplemented with 100 ng ml^{-1} anhydrotetracycline. Cross-out mutants were determined by PCR using primers targeting the two flanking regions of the indicated genes. PCR of an intact gene plus its flanking regions yielded a product of approximately 1,150–1,500 bp, whereas successful deletion of the gene of interest resulted in a PCR amplicon of only 350–450 bp of its two flanking regions.

Proteome analysis of ileal contents

Proteins in the ileal contents were extracted by pipetting and inverting in Tris-buffered saline with Tween 20 (TBST) with protease inhibitors (APExBIO, K1007). Insoluble material was removed by centrifugation at 12,000*g* for 20 min at 4 °C. The supernatant was then transferred to a separate tube and 25% trichloroacetic acid (final concentration 12.5% (v/v)) was added. The mixture was incubated for 1 h at 4 °C. After centrifugation at 12,000*g* for 15 min at 4 °C to remove the supernatant, the precipitate was cleaned twice with acetone and allowed to dry with the lid open. Using a water bath sonicator, the dried material was redissolved in 0.5% sodium dodecanoate and 100 mM Tris-HCl, pH 8.5. The redissolved sample was assayed for protein concentration using the BCA assay and the protein concentration was adjusted to 1 μg μl^{-1}. Peptides were then collected after protein digestion by trypsin and desalination. Nanoflow liquid chromatography–tandem mass spectrometry (LC–MS/MS) analysis of tryptic peptides was conducted on a quadrupole Orbitrap mass spectrometer (Q Exactive HF-X, Thermo Fisher Scientific) coupled to an EASY nLC 1200 ultra-high pressure system (Thermo Fisher Scientific) by means of a nano-electrospray ion source. Peptides (500 ng) were loaded on a 25-cm column (150-μm inner diameter, packed using ReproSil-Pur C18-AQ 1.9-μm silica beads). Peptides were separated using a gradient from 8% to 12% B in 5 min, then 12% to 30 % B in 33 min and stepped up to 40% in 7 min followed by a 15-min wash at 95% B at 600 nl min^{-1}, in which solvent A was 0.1% formic acid in water and solvent B was 80% acetonitrile (ACN) and 0.1% formic acid in water. The total duration of the run was 60 min. Column temperature was kept at 60 °C using an in-house-developed oven. Briefly, the mass spectrometer was operated in 'top-40' data-dependent mode, collecting mass spectrometry (MS) spectra in the Orbitrap mass analyser (120,000 resolution, 350–1,500 m/z range) with an automatic gain control target of 3×10^6 and a maximum ion injection time of 80 ms. The most intense ions from the full scan were isolated with an isolation width of 1.6 m/z. Following higher-energy collisional dissociation with a normalized collision energy of 27, MS/MS spectra were collected in the Orbitrap (15,000 resolution) with an automatic gain control target of

5×10^4 and a maximum ion injection time of 45 ms. Precursor dynamic exclusion was enabled with a duration of 16 s.

RAW data files were processed and quantified using Proteome Discoverer software v.2.4.1.15 (Thermo Fisher Scientific) and searched against the RefSeq mouse protein database (UP000000589, 55,260 sequences, release 2023_03) using the SEQUEST algorithm. The following search parameters were used: fixed modifications, including carbamidomethylation of cysteine (+57.02146 Da); variable modification, including oxidation of methionine (+15.99492 Da). The mass tolerance for precursor ions was 20 ppm, and fragment ions were set to ±0.05 Da. Trypsin was set as the enzyme, allowing for two missed cleavages. Searches used a reverse sequence decoy strategy to control peptide false discovery, and identifications were validated using Percolator software (v.3.06.1), with an FDR of 0.01 for proteins and peptide spectrum matches. For protein quantification, background correction was checked and then median normalization was applied. For quantification, proteins with at least one unique peptide were considered for further analysis.

Recombinant protein purification

Mouse APOL9a, APOL9b or *B. thetaiotaomicron* ceramide kinase (BT_0871), including either the wild-type form or a catalytic domain deletion mutant lacking the conserved GGDG motif (Δ65-68)[48], was expressed as a C-terminal 6 × His-tagged fusion protein using the pET-28a vector in BL21 (DE3) chemically competent cells (TSINGKE, TSC-E01). Bacteria were cultured in Luria-Bertani (LB) supplemented with kanamycin (50 μg ml^{-1}) overnight, then the cultures were diluted 1:100 in fresh LB to grow to optical density $(OD)_{600} = 0.6$, followed by induction with 1 mM isopropyl β-D-1-thiogalactopyranoside (IPTG) (Sango Biotech, A100487) for 20 h at 20 °C. Bacteria were then collected by centrifugation and resuspended in binding buffer (20 mM sodium phosphate, 0.5 M NaCl, 100 μg ml^{-1} lysozyme, 10 U ml^{-1} DNase I, 1 mM phenylmethylsulfonyl fluoride (PMSF), 20–40 mM imidazole, pH 7.4) for 30 min on ice and lysed by sonication. Insoluble material was pelleted at 20,000*g*, and the solubilized protein in the supernatant was affinity purified using HisTrap FF crude (cytiva, 11000458), followed by elution using a 50–500 imidazole gradient. After the binding buffer was replaced with PBS supplemented with 1 mM PMSF by extensive dialysis (more than 3 buffer changes of at least 1,000-fold v/v), the dialysed protein was preserved in PBS supplemented with 10% glycerol and 1 mM PMSF and then stored at −80°C.

For purification of human APOL1–APOL4 proteins, full-length APOL1, APOL2, APOL3 and APOL4 protein sequences were cloned into pFastBac plasmids with a C-terminal Flag tag. Individual plasmids were transformed into DH10Bac competent cells (Biomed, BC112-01) and plated on an LB agar plate containing 50 μg ml^{-1} kanamycin, 7 μg ml^{-1} gentamicin, 10 μg ml^{-1} tetracycline, 100 μg ml^{-1} X-gal and 40 μg ml^{-1} IPTG. After 48 h of incubation at 37 °C, the white spot colonies were picked for colony PCR identification. Positive colonies were cultured in liquid LB medium containing 50 μg ml^{-1} kanamycin, 7 μg ml^{-1} gentamicin and 10 μg ml^{-1} tetracycline. Bacmid DNA was extracted using the TIANprep Mini Plasmid Kit (TIANGEN, DP103) and precipitated with isopropanol. Sf9 cells were cultured using ESF921 Insect Cell Culture Medium (Expression Systems, 96-001-01). Bacmid DNA was transfected into Sf9 insect cells using X-tremeGENE 9 DNA Transfection Reagent (Roche, 6365779001). Transfected cells were incubated at 28 °C in a shaker incubator at 135 rpm for 72 h and the supernatant containing recombinant baculovirus (P0) was collected. For baculovirus amplification, 3 ml of P0 was infected into 30 ml of Sf9 cells (2–2.5 × 10^6 cells per ml) and incubated at 28 °C in a shaker incubator at 135 rpm for 48 h, and the supernatant (P1) was collected. For protein expression, 10 ml of P1 was infected into 1 l of Sf9 cells (2–2.5 × 10^6 cells per ml) and incubated at 28 °C in a shaker incubator at 135 rpm for 48 h. Infected cells were collected by centrifugation and resuspended in lysis buffer (50 mM HEPES, 150 mM NaCl, 1 mM DTT, 10 U ml^{-1} DNase I, 1 × protease inhibitor cocktail, 1% *n*-dodecyl-β-D-maltopyranoside (DDM)). Cells were lysed at 4 °C at 140 rpm for 2 h and centrifuged at 40,000*g* for 30 min, and the supernatant was collected. Then, 1 ml of anti-flag beads (GenScript, L00432) was added to the supernatant and incubated at 4 °C at 140 rpm for 2 h, and the indicated APOL protein was eluted with FLAG peptide (200 μg ml^{-1}) in competitive elution buffer (50 mM HEPES, 150 mM NaCl, 1 mM DTT, 1 × protease inhibitor cocktail, 1% DDM, 0.1% cholesteryl hemisuccinate Tris salt). Protein concentrations were determined by BCA assay. The purified protein was stored in Tris-buffered saline (TBS) with 10% glycerol at −80 °C until further use.

Faecal microbiota collection for mass spectrometry or flow cytometry

For the collection of ileal microbiota for mass spectrometry analysis or flow cytometry after APOL9 binding, procedures were performed as previously described with minor modifications[20]. In brief, an approximately 6–8-cm-long ileum was isolated from killed mice. Mucus and luminal contents were collected and transferred to the homogenization tube, followed by incubation with 1 ml of PBS on ice for 15 min (the protease inhibitor cocktail was required for MS analysis). Then, 0.25 μg of grinding beads were added and vortexed continuously for at least 3 min until the stool sample was thoroughly homogenized. After homogenization, large insoluble particles were removed by centrifugation for 10 min at 50*g*, 4 °C. For MS analysis, the faecal bacteria in the supernatants were transferred to new tubes and centrifuged for 5 min (8,000*g*, 4 °C) before being resuspended in 1 ml of PBS and then filtered through 5-μm filters (Millipore, SVLP02500). Bacterial pellets were then further collected and lysed in 1 × SDS loading buffer (2% SDS, 10% glycerol, 100 mM DTT, 0.1% bromophenol blue and 50 mM Tris-HCl pH 6.8). These samples were then subjected to SDS–PAGE and in-gel digestion.

For flow cytometry analysis, faecal bacteria in the supernatants were centrifuged for 3 min (8,000*g*, 4 °C) and washed with 1 ml of PBS containing 1% (w/v) BSA (staining buffer, YEASEN). This step was repeated twice before resuspension in 1 ml of staining buffer. One sample of this bacterial suspension (100 μl) was saved as a presort sample for 16S sequencing analysis. The remaining faecal bacterial suspensions were divided into 100 μl per sample and stained with SYTO BC (5 μM, Thermo Fisher Scientific, S34855) for 15 min on ice, followed by incubation with recombinant APOL9a protein (0.1 μg ml^{-1}) for 30 min on ice. After washing with 500 μl of PBS, the bacterial pellets were stained with 100 μl of staining buffer containing anti-APOL9 antibody (1 μg ml^{-1}) for 30 min on ice. After a further wash, the bacterial pellets were resuspended in 100 μl of staining buffer containing PE-conjugated donkey anti-rabbit IgG antibody (1:50, BioLegend). Samples were then washed three times with 1 ml of staining buffer before flow cytometric analysis or cell separation (see Supplementary Fig. 1 for detailed gating strategies).

Phylogenetic analysis of Cer1P biosynthesis genes in the gut microbiome

Amino acid sequences of four enzymes involved in Cer1P synthesis (Kyoto Encyclopedia of Genes and Genomes (KEGG) IDs: BT_0870, BT_3075, BT_3032 and BT_0871) were retrieved from the KEGG database. These sequences were used to search the genomes of 52 gut-derived bacterial strains using BLASTp (v.2.16.0), with an e-value threshold of less than 10^{-5} and a minimum identity of 20% or 40%. To assess their distribution in human populations, the healthy human gut metagenomic datasets ($n = 361$) from the iHMP dataset were analysed[36]. Quality control and assembly of raw sequencing reads into contigs were performed using the Sunbeam pipeline[49]. Genomic binning was performed using MetaBAT2[50], and taxonomy was assigned using CheckM[51]. Homologous genes within the metagenome-assembled genomes were identified using BLASTp with the same search criteria.

Lipid extraction and lipidomics analysis

Lipids were extracted from *B. thetaiotaomicron* using a modified version of that previously described[52]. In brief, *B. thetaiotaomicron* were

homogenized in 900 µl of chloroform/methanol/MilliQ H_2O (3:6:1) (v/v/v). The homogenate was then incubated at 1,500 rpm for 30 min at 4 °C. At the end of the incubation, 350 µl of deionized water and 300 µl of chloroform were added to induce phase separation. The samples were then centrifuged and the lower organic phase containing lipids was extracted into a clean tube. Lipid extraction was repeated once by adding 500 µl of chloroform to the remaining aqueous phase, and the lipid extracts were combined in a single tube and dried in the SpeedVac in OH mode. The samples were stored at −80 °C until further analysis.

Lipidomic analyses were performed at LipidALL Technologies using a Shimadzu Nexera 20AD-HPLC coupled to a Sciex QTRAP 6500 PLUS as previously reported[52]. Separation of individual lipid classes of polar lipids by normal phase HPLC was performed using a TUP-HB silica column (internal diameter 150 × 2.1 mm^2, 3 µm) with the following conditions: mobile phase A (chloroform/methanol/ammonium hydroxide, 89.5:10:0.5) and mobile phase B (chloroform/methanol/ammonium hydroxide/water, 55:39:0.5:5.5). Multiple reaction monitoring (MRM) transitions were set up for comparative analysis of different polar lipids. Individual lipid species were quantified by reference to spiked internal standards. Cer d18:1/15:0-d7, d3-LacCer d18:1/16:0 were purchased from Avanti Polar Lipids.

Affinity isolation of lipids by recombinant APOL9a protein

Lipid immunoprecipitation was performed as previously described with modifications[53]. In brief, 100 µl of Ni-charged MagBeads (GenScript, L00295) were washed three times with sterile, filtered PBS and resuspended in binding buffer (20 mM Tris-HCl, 150 mM NaCl, 5 mM imidazole, 0.1% Triton X-100, 1 mM PMSF and protease inhibitors). His-tagged recombinant APOL9a (5 µg ml^{-1}) was added to the beads, followed by incubation at 4 °C for 4 h with gentle shaking. Dried lipid extracts (10 µg) from *B. thetaiotaomicron* were rehydrated in 800 µl of the binding buffer by gentle sonication and then added to the protein-bound beads. The mixture was incubated for 1 h at room temperature with gentle rotation. Beads without protein binding were used as a negative control. The resin was washed three times with washing buffer (binding buffer + 20 mM imidazole) to remove unbound components. Lipid–protein complexes were eluted with 200 µl of PBS containing 500 mM imidazole. The eluted fractions were collected, and lipids were extracted by adding 600 µl of chloroform/methanol (2:1, v/v). The samples were vortexed for 5 min and then spun at 2,000*g* for 15 min to separate the aqueous and organic phases. The lower organic phase was transferred to a pre-weighed thin-walled glass vial and dried in a vacuum concentrator and resuspended in a suitable solvent for subsequent LC–MS/MS analysis.

Ceramide kinase assay

The ceramide kinase assays were performed similarly as previously described for human CERK[34,48]. In brief, the reaction was performed in a 60-µl buffer containing 20 mM HEPES (pH 7.4), 10 mM KCl, 15 mM $MgCl_2$, 10% glycerol, 1 mM DTT, 1 mM ATP, 0.2 mg ml^{-1} fatty acid-free BSA and 50 ng $µl^{-1}$ purified *B. thetaiotaomicron* ceramide. The reaction was started by adding 0.025 µg $µl^{-1}$ of the recombinant *B. thetaiotaomicron* ceramide kinase enzyme (BT_0871). Kinase-dead BT_0871 enzyme was used as a control. Tubes were incubated in a water bath at 30 °C for 1 h. After the incubation, reactions were stopped and lipids were extracted by adding 180 µl of chloroform/methanol (2:1, v/v). After vortexing, the phases were separated by centrifugation. The lower solvent layer was collected, transferred to a new tube and dried using a high-speed vacuum concentrator.

TLC of lipids

Lipid extracts were applied to silica HPTLC plates (silica gel HSGF254, 2.5 × 5 cm^2, 0.2-mm layer thickness), with loading volumes normalized to the OD_{600} of the original cultures. The plates were developed using a standard lipid extraction solvent system of 70:20:5 (v/v/v, for total lipid extracts) or 65:25:4 (v/v/v, for lipid extracts after kinase assay) chloroform/methanol/ammonium hydroxide (25% NH_3 basis). The d18:1/16:0 ceramide (Cayman, 10681) was used as a lipid standard. After development, the plates were sprayed with primuline solution (0.1 mg ml^{-1} in 4:1 v/v acetone/distilled H_2O) and visualized under ultraviolet light at 365 nm (ref. 35). For further lipid separation and analysis by LC–MS/MS or protein–lipid overlay assays, lipid bands were stained with iodine vapour (for ceramides) or phosphomolybdic acid staining (for Cer1Ps). After visualization, lipid fractions were scraped from the plate with razor blades and transferred to 2-ml round-bottomed Eppendorf tubes. Lipids were re-extracted by the method as described above. To remove potential phospholipid contaminants and obtain relatively purified ceramides, the ceramide extracts were subjected to mild alkaline hydrolysis using 0.1 M methanolic potassium hydroxide at 37 °C for 1 h in a water bath before extraction. The dry weight of the lipid extracts was determined using an electronic analytical balance before and after lyophilization.

Protein–lipid overlay assay

Lipid binding assays were performed using lipid-coated nitrocellulose membranes as previously described[54]. Membranes pre-spotted with different lipid species (50 ng $µl^{-1}$) were blocked with 3% fatty acid-free BSA in TBST for 1 h at room temperature. After blocking, the membranes were incubated with recombinant APOL9a, APOL9b or APOL2 protein (~100 ng ml^{-1}) prepared in 3% fatty acid-free BSA in TBST for 3 h at room temperature. Binding was detected using a primary anti-APOL9 or anti-Flag (for Flag-tagged APOL2) antibody, followed by an HRP-conjugated goat anti-rabbit secondary antibody. Signals were visualized using enhanced chemiluminescence and imaged accordingly.

IEC isolation and culture

For RNA or protein collection, ileal tissues were isolated from killed mice. After removal of the remaining mesentery/fat and Peyer's patches, the tissues were opened longitudinally and washed three times with cold PBS. The tissues were then cut into 1-cm pieces and then shaken with pre-warmed 1640 RPMI containing 1 mM DTT, 5 mM EDTA, 100 U ml^{-1} penicillin, 100 µg ml^{-1} streptomycin and 5% fetal bovine serum (FBS) for 15 min at 200 rpm, 37 °C. The supernatants were then collected and filtered through 70-µm cell strainers before being further used.

For in vitro culture, small intestine tissues were isolated from 4-week-old killed mice and opened longitudinally. The mucosal villi were carefully scraped off and the remaining tissues were washed three times with ice-cold PBS. After the small intestine was cut into 2-cm pieces, the tissues were placed in a 50-ml centrifuge tube and remixed with 25 ml of ice-cold PBS containing 1% v/v FBS, 100 U ml^{-1} penicillin, 100 µg ml^{-1} streptomycin and 2 mM EDTA. The tubes were then immersed in ice and shaken twice at 120 rpm for 12 min in an orbital shaker. After discarding the supernatant, the remaining tissues were resuspended in 20 ml of ice-cold PBS and then shaken vigorously by hand for 1 min. The supernatants were then collected and transferred to a new 50-ml centrifuge tube. Cells and small sheets of intestinal epithelium were separated from the denser intestinal fragments by collecting supernatants after two 60-s sedimentations at 1*g*. To discard the monodispersed IECs, non-IECs and debris, cells were centrifuged three times at 150*g* for 3 min in DMEM plus 2% sorbitol. After the final centrifugation, the IEC-containing pellets were resuspended in complete growth media (Advanced DMEM/F-12, 5% v/v FBS, 100 U ml^{-1} penicillin, 100 µg ml^{-1} streptomycin, 10 ng ml^{-1} mouse epidermal growth factor, 2 mM GlutaMAX, 10 mM HEPES, 1 × N2 supplement, 1 × B27 supplement and 50% L-WRN conditioned medium). Then, 200 µl of cell suspension was seeded into the 48-well plate precoated with 2% Matrigel and cultured in a cell incubator (5% CO_2, 37 °C). The culture medium was changed after 3–6 h to remove non-adherent cells. Adherent cells were incubated overnight for follow-up experiments.

Gut IEL, LPL and spleen DC isolation

IELs and LPLs were isolated as previously described with modifications[55]. In brief, the small intestine was opened longitudinally and washed three times with PBS containing 0.1% BSA, 100 U ml^{-1} penicillin and 100 μg ml^{-1} streptomycin. After removal of the remaining mesentery/fat and Peyer's patches, the specimen was cut into 1-cm pieces and then shaken with pre-warmed 1 × Hanks' balanced salt solution media (without Ca^{2+} and Mg^{2+}) containing 1 mM DTT, 5 mM EDTA, 100 U ml^{-1} penicillin, 100 μg ml^{-1} streptomycin and 5% FBS for 30 min at 200 rpm, 37 °C. The supernatants were then collected and filtered through 70-μm cell strainers before separation on a 40–80% Percoll density gradient (GE Healthcare, 17-0891-01). Cells layered between the 40–80% fractions were collected as IELs. For LPL isolation, the epithelial cell layer was removed as described above and the remaining intestinal tissues were washed twice with RPMI 1640 culture medium. The tissues were then digested in RPMI 1640 supplemented with 1 mg ml^{-1} collagenase type I (17100017, Thermo Fisher Scientific), 0.1 mg ml^{-1} DNase I (Roche, 10104159001) and 5% FBS at 200 rpm at 37 °C for 30 min. The released cells were then filtered through 40-μm cell strainers, followed by Percoll fractionation to isolate LPLs as described above.

For isolation of splenic DCs, whole spleens were cut into 2-mm^2 pieces and digested at 200 rpm for 30 min at 37 °C in 2 ml of RPMI 1640 containing 0.5 mg ml^{-1} collagenase IV (Sigma, C5138), 10% v/v FBS and 0.01 mg ml^{-1} DNase I. The cell suspension was then passed through a 40-μM filter and centrifuged at 500*g* for 3 min. DCs were first enriched with CD11c microbeads (Miltenyi, 130-125-835).

Flow cytometry and cell sorting

Suspensions of lymphocytes, DCs or IECs were prepared by sieving and gentle pipetting. Cells were then washed with ice-cold FACS buffer (2% FBS and 2 mM EDTA in PBS) and subsequently stained with appropriate antibodies for 30 min. Antibodies for flow cytometry were purchased from Thermo Fisher Scientific or BioLegend as follows: CD45-FITC (11-0451-82, 30-F11, 1:200) and -EFLUOR 450 (48-0451-82, 30-F11, 1:200); TCR-γδ-PE (12-5711-82, GL3, 1:200) and -PE-Cy7 (25-5711-82, GL3, 1:200); TCR-β-FITC (11-5961-82, H57-597, 1:200) and -PerCP-Cyanine5.5 (45-5961-82, H57-597, 1:200); CD8α-FITC (11-0081-82, 53-6.7, 1:200), -PE-Cy7 (25-0081-82, 53-6.7, 1:200) and -APC (17-0081-82, 53-6.7, 1:200); CD8β-FITC (11-0083-82, EBIOH35-17.2, 1:200), -PE (12-0083-82, EBIOH35-17.2, 1:200) and -APC (17-0083-81, EBIOH35-17.2, 1:200); CD4-PE (12-0042-82, RM4-5, 1:200) and -APC (17-0042-82, RM4-5, 1:200); CD11c-APC (17-0114-82, N418, 1:200); CD3ε-FITC (11-0031-82, 145-2C11, 1:200), -PE (12-0031-82, 145-2C11, 1:200) and -APC (17-0031-82, 145-2C11, 1:200); FOXP3-PE (12-5773-82, FJK-16s, 1:100); RORγt-APC (17-6981-82, B2D, 1:100); IL-17-APC (17-7177-81, eBio17B7, 1:100); IFNγ-PE (12-7311-82, XMG1.2, 1:100); MHC-II-PE-Cy7 (25-5321-82, M5/114.15.2, 1:200); Epcam-APC (17-5791-82, 2E7, 1:200). After washing twice with FACS buffer, DAPI (1:1,000) was added to single-cell suspensions 5 min before sorting to exclude dead cells. Stained cells were analysed on a Beckman Gallios flow cytometer or sorted on a Beckman Moflo Astrios. Intracellular staining was performed according to the protocol of the Foxp3/Transcription Factor Staining Buffer set (Thermo Fisher Scientific, 00-5523-00). FlowJo_V10 software (v.10.0.7) was used for data analysis. The gating strategy for different cell sorting was shown as follows: $DAPI^-Epcam^+CD45^-$ for total small intestine epithelial cells; $DAPI^-CD45^+CD3^+$ for total small intestine IELs; $DAPI^-CD45^+CD11c^+MHC\text{-}II^+$ for DCs (see Supplementary Fig. 1 for detailed gating strategies).

Co-housing, microbiota depletion and reconstitution

The procedures for the co-housing and microbiota reconstitution experiments were performed as previously reported[56]. For co-housing experiments, germ-free and SPF wild-type mice, age- and sex-matched to approximately 4 weeks of age, were randomized and housed in the same room in an isolator cage with the same diet for at least 4 weeks. For microbiota reconstitution experiments, GF mice were transferred to new isolator cages and given orally 200 μl of faecal bacteria obtained by homogenizing the entire contents of the faeces of matched donor mice in 50 ml of water. For microbiota depletion, the drinking water of the indicated mice was supplemented with a weekly mixture of 1 g l^{-1} ampicillin, metronidazole, neomycin sulfate and 0.5 g l^{-1} vancomycin hydrochloride (Sangon Biotech) for 4 weeks. Changes in caecum size caused by bacterial death and a stool DNA extraction kit to assess faecal bacterial 16S rDNA were used to measure ABX activity. For FMT in SPF mice, the mice were pre-treated with the same broad-spectrum ABX for 1–2 weeks before transplantation of donor ileal microbiota lacking Bacteroidales. FMT with either wild-type or BT_0871-deficient *B. thetaiotaomicron* was performed using bacteria grown anaerobically for 48 h on blood agar plates from frozen stocks. Single colonies were inoculated into BHIS medium, and the cultures were collected after 18 h. Bacterial cultures were quantified by OD measurement, pelleted and resuspended in PBS (5 ml of culture resuspended in 500 μl of sterile PBS). The bacterial suspension was then mixed with faecal bacteria at an OD ratio of approximately 2:3 and administered to mice by oral gavage (200 μl per mouse). Colonization status was verified by qPCR analysis.

Immunoblotting

For protein extraction from primary IECs, cells were collected from the indicated mice as described above, washed twice with ice-cold PBS and then lysed for 30 min on ice with RIPA lysis solution (Beyotime, P0013) containing 1 mM PMSF and protease inhibitors. The lysates were then centrifuged at 13,000*g* for 15 min at 4 °C. Protein concentration was determined by the Bradford method. During the pre-run, the supernatant was boiled with 2 × PAGE loading buffer 1:1 (v/v) containing 125 mM Tris-HCl pH 6.8, 30% glycerol and 0.1% bromophenol blue in ddH_2O for 10 min, and then followed by SDS–PAGE analysis (see Supplementary Fig. 2 for uncropped immunoblotting images).

Real-time PCR

RNAs were extracted from cells or tissues using RNAiso reagent (Takara, 9109) according to the manufacturer's instructions, and then reverse transcribed into complementary DNA using the One-Step PrimeScript RT-PCR Kit (Takara, RR037A). The cDNAs were used for real-time PCR analysis with the indicated primer sets and SYBR Green PCR Master Mix (YEASEN, 11202ES03). PCR was performed using Step One Plus Real-Time PCR Systems (VIIA7, Applied Biosystems). The PCR conditions were 95 °C for 1 min, followed by 40 cycles of denaturation at 95 °C for 5 s and annealing and extension at 60 °C for 30 s. The primers used are listed in Supplementary Table 9.

Immunofluorescence

For tissue immunofluorescence, unwashed mouse ileal tissues (including luminal contents) were fixed in Carnoy's fixative consisting of 60% methanol, 30% chloroform and 10% acetic acid at 4 °C overnight, followed by embedding in paraffin as described[57]. Next, 8-μm sections were cut, dewaxed and hydrated. The sections were then blocked with 1% BSA in PBS for 1 h and subjected to immunostaining. The antibodies and stains used for immunofluorescence were as follows: rabbit anti-APOL9 (1:200), donkey anti-rabbit IgG secondary antibody, Alexa Fluor 594 (Thermo Fisher Scientific, A21207, 1:1,000), DAPI (1:1,000, Beyotime), rhodamine-conjugated UEA1 (Ulex Europaeus Agglutinin 1, Vector Laboratories, 1:500). Tissues were visualized by fluorescence microscopy (Zeiss Axio Imager A2). To visualize APOL9/APOL2 binding to *B. thetaiotaomicron* by immunofluorescence, recombinant mouse APOL9a/b or human APOL2 was labelled with sulfo-Cyanine3 NHS ester (D10016, Duofluor) and overnight bacterial cultures were stained with SYTO BC Green dyes (5 μM) according to the manufacturer's instructions. Cy3-labelled APOL9 or APOL2 was then incubated with SYTO-labelled *B. thetaiotaomicron* at a final concentration of

5 μg ml^{-1} for 20 min in an anaerobic chamber. The mixture was centrifuged, washed once with PBS and resuspended in PBS. Slides were then mounted and observed using a Zeiss LSM880NLO FLIM microscope. Data were analysed by ZEN software (Zeiss, black edition, v.1.1.0.0).

Bacterial killing assays

Bacterial killing assays were performed as previously described with minor modifications[16]. Briefly, 5 ml of bacterial cultures were grown to the midlogarithmic phase, and then pelleted and washed in 5 ml of standard assay buffer (10 mM MES pH 5.5 and 25 mM NaCl). Purified APOL9 proteins were added at various concentrations (0–30 μg ml^{-1}) to around 5×10^6 c.f.u. per ml of bacteria. Bacteria were incubated at 37 °C for 2 h and then washed in PBS, and stained with 1 μg ml^{-1} propidium iodide in PBS for 20 min. The cells were then centrifuged and washed in PBS. A flow cytometer was used to determine the percentage of propidium iodide-positive cells (CytoFLEX, Beckman).

16S rRNA gene sequencing

Total genomic DNA from microbial samples was extracted using the QIAamp Fast DNA Stool Mini Kit (QIAGEN) according to the manufacturer's protocols. DNA concentration was monitored using the Qubit dsDNA HS Assay Kit. Next-generation sequencing libraries and Illumina sequencing were performed by the company (AZENTA). The sequencing library was prepared using the MetaVX Library Preparation Kit. Briefly, 20–50 ng of DNA was used to generate amplicons covering the V3 and V4 hypervariable regions of the bacterial 16S rRNA gene (the forward primer: 'CCTACGGRRBGCASCAGKVRVGAAT'; and the reverse primer: 'GGACTACNVGGGTWTCTAATCC'). The amplicon concentration was detected by a microplate reader (Tecan, Infinite 200 Pro) and the approximately 600-bp amplicon fragment was detected by 1.5% agarose gel electrophoresis. Then, 250/300-bp paired-end sequencing was performed using an Illumina MiSeq/NovaSeq platform (Illumina) following the manufacturer's protocols. After dual-indexed sequencing, paired-end reads were merged and filtered to remove sequences containing ambiguous bases (N), retaining sequences with lengths greater than 200 bp. Following quality filtering and chimera removal, the remaining sequences were clustered into operational taxonomic units (OTUs) using VSEARCH (v.1.9.6) at a 97% similarity threshold, with the SILVA 138 database as the 16S rRNA reference. The representative OTU sequences were taxonomically classified using the RDP classifier (Ribosomal Database Program) with a Bayesian algorithm, and the community composition of each sample was analysed at different taxonomic levels. Beta diversity was assessed by means of unweighted UniFrac analysis to evaluate significant differences between microbial communities. Visualization was performed using PCA on the basis of OTU abundance. Hierarchical clustering was conducted using the UPGMA (unweighted pair group method with arithmetic mean) algorithm with the group average linkage method.

RNA-seq of *B. thetaiotaomicron*

RNA purification, cDNA library preparation and sequencing. Total bacterial RNA was extracted from each sample using the RNeasy Mini Kit (Qiagen). The extracted RNA was quantified and assessed for quality using an Agilent 2100/2200 Bioanalyzer, a NanoDrop spectrophotometer (Thermo Fisher Scientific) and 1% agarose gel electrophoresis. Approximately 300–500 ng of total RNA was then hybridized with a single-stranded DNA probe designed to target rRNA. After hybridization, both the rRNA and the bound DNA probe were digested to remove them from the mixture. The remaining RNA was purified using RNA Clean Beads for recovery. The purified RNA was fragmented using divalent cations to generate suitable templates for library preparation. Reverse transcription was performed using random primers to synthesize cDNA from the fragmented RNA. During the second-strand synthesis, dUTP (deoxyuridine triphosphate) was incorporated, while 5′ phosphorylation and 3′ adenylation were performed simultaneously in the same reaction. Sequencing adaptors were then ligated to both ends of the double-stranded cDNA to allow identification and sequencing during downstream processes. The adaptor-ligated fragments were purified and size selected using DNA Clean Beads to enrich the desired library fragments. Next, PCR amplification was performed using P5 and P7 primers to generate the final library. Uracil-DNA glycosylase was included in the PCR mix to degrade the dUTP-containing second strand and ensure strand specificity. Rigorous quality control checks were performed to confirm the suitability of the library for sequencing. Finally, libraries from different samples, each uniquely indexed, were pooled and sequenced using paired-end 150-bp (PE150) sequencing on an Illumina NovaSeq 6000 platform following the manufacturer's instructions.

Data analysis. To remove technical sequences, such as adaptors, PCR primers or their fragments, and poor quality bases (Phred score <20), the raw FASTQ data were processed using Cutadapt (v.1.9.1). The parameters used included a Phred cutoff of 20, an error rate of 0.1, a minimum adaptor overlap of 1 bp, a minimum read length of 75 bp and a maximum N ratio of 0.1. First, reference genome sequences and gene model annotation files for the relevant species were downloaded from the genome databases of UCSC, NCBI and ENSEMBL. The reference genomes were then indexed using Bowtie2 software (v.2.2.6). Clean reads were then aligned to the indexed reference genome using Bowtie2 with default parameters. For transcript quantification, transcripts in FASTA format were generated from known GFF annotation files and properly indexed. Using this as a reference, gene expression levels were estimated from the paired-end clean data by HTSeq (v.0.6.1p1). Differential expression analysis was performed using the DESeq2 package in Bioconductor, which uses a model based on the negative binomial distribution. To control the FDR, *P* values were adjusted using the Benjamini–Hochberg method, and genes with adjusted *P* values <0.05 were considered differentially expressed. For functional enrichment analysis, GOSeq (v.1.34.1) was used to identify Gene Ontology terms associated with enriched genes, with a significance threshold of $P < 0.05$.

Bulk RNA-seq. Total RNA was extracted from the tissues using TRIzol reagent according to the manufacturer's instructions. RNA quality was then determined using the 5300 Bioanalyzer (Agilent) and quantified using the ND-2000. Only high-quality RNA samples (RNA Integrity Number ≥8) were used for sequencing library construction. RNA purification, reverse transcription, library construction and sequencing were performed at Shanghai Majorbio Bio-pharm Biotechnology (Shanghai, China) according to the manufacturer's instructions (Illumina). The transcriptome library was prepared according to Stranded mRNA Prep and Ligation from Illumina using 1 μg of total RNA. Briefly, messenger RNA was isolated using the polyA selection method with oligo (dT) beads and then fragmented using a fragmentation buffer. Second, double-stranded cDNA was synthesized using a SuperScript double-stranded cDNA synthesis kit (Invitrogen) with random hexamer primers (Illumina).

The synthesized cDNA was then subjected to end repair, phosphorylation and 'A' base addition according to Illumina's library construction protocol. Libraries were size selected for cDNA target fragments of 300 bp on 2% Low Range Ultra Agarose, followed by PCR amplification using Phusion DNA Polymerase (NEB) for 15 PCR cycles. After quantification using Qubit 4.0, the paired-end RNA-seq library was sequenced on the NovaSeq 6000 sequencer (2 × 150-bp read length). Raw paired-end reads were trimmed and quality controlled using fastp with default parameters. Clean reads were then aligned separately to the reference genome in orientation mode using HISAT2 software. The mapped reads of each sample were assembled using StringTie in a reference-based approach. To identify differential expression genes between two different samples, the expression level of each transcript was calculated using the transcripts per million reads method. RSEM was used to quantify

gene abundance. Essentially, differential expression analysis was performed using DESeq2 or DEGseq. Differential expression genes with $|\log_2FC| \geq 1$ and FDR ≤ 0.05 (DESeq2) or FDR ≤ 0.001 (DEGseq) were considered significantly differentially expressed genes.

scRNA-seq. The prepared cell suspension was counted using a TC20 Automated Cell Counter (Bio-Rad) to obtain information on cell size, concentration and viability, and to determine the sample loading volume. Libraries were constructed using Chromium Single Cell 3′ Library (10× Genomics) & Gel Bead Kit V2 (10× Genomics) according to the manufacturer's instructions. Subsequently, libraries with different indices were multiplexed and loaded onto an Illumina NovaSeq instrument according to the manufacturer's instructions. Sequencing was performed using a 2 × 150-bp paired-end configuration; image analysis and base calling were performed using the NovaSeq Control Software + OLB + GAPipeline-1.6 (Illumina) on the NovaSeq instrument.

The pipelines of CellRanger (v.7.1.0) were used to analyse the sequencing data generated by Chromium Single Cell Gene Expression. Data normalization, dimensional reduction, cell clustering and differential expression analysis were performed using the R package Seurat (v.4.1.1). For quality control, genes detected in fewer than three cells were excluded from the merged counting matrix. Cell filtering thresholds were determined on the basis of data distribution and expression patterns. Cells with expressed genes below 800 or above 6,000 were excluded to avoid empty droplets or doublets. Cells with a mitochondrial gene count greater than 10% were also excluded to ensure cell quality. Cell clusters overexpressing markers of two cell types were considered potential doublet clusters and removed from the analysis.

The filtered expression matrix contained 25,178 cells and 21,033 genes. Data normalization was performed using the Seurat NormalizeData function. Identification of 2,000 highly variable genes was performed using the FindVariableFeatures function, followed by data scaling using the ScaleData function. PCA was performed using the RunPCA function for linear dimension reduction. The *t*-SNE was then performed using the top 50 principal components using the RunTSNE function. For cell clustering, a shared nearest neighbour graph was generated using the FindNeighbors function, and clustering was performed using the FindClusters function with a resolution of 1.2. Annotation of cell clusters was achieved by referencing known marker genes from the Lusis lab publication[58] and the CellMarker database. To identify differentially expressed genes between cell types and between treatment and control within each cell type, Wilcoxon tests were performed using the FindMarkers function.

Isolation, quantification and size measurement of bacterial OMVs. *B. thetaiotaomicron* VPI-5482 was cultured in BHIS broth overnight at 37 °C under anaerobic conditions. The culture supernatant was then collected by centrifugation at 11,000*g* for 10 min at 4 °C to remove bacterial pellets. The supernatant was then filtered through 0.45-μm filters and ultracentrifuged at 400,000*g* for 1 h at 4 °C in a 70-Ti rotor (Beckman). The concentrated pellets were resuspended in PBS and stored at −80 °C for further use. The number and average size of *B. thetaiotaomicron* OMVs were measured by nanoparticle tracking analysis (RESUN-E03).

***Bacteroides* OMV production induced by recombinant APOL proteins.** *B. thetaiotaomicron* VPI-5482, *B. fragilis* NCTC 9343, *B. vulgatus* ATCC 8482 or *P. goldsteinii* ATCC BAA-1180 was cultured in BHIS broth overnight at 37 °C under anaerobic conditions, then inoculated into 5 ml of BHIS broth medium at a 1:50 dilution and grown at 37 °C to mid-log phase (OD_{600}, approximately 1). After centrifugation at 8,000*g* for 3 min, the cells were resuspended with fresh 37 °C BHIS broth, and 400 μl of bacterial suspension was transferred to new 1.5-ml Eppendorf tubes. BSA was added as a negative control, and mouse APOL9a/b and human APOL2 were added to final concentrations of 5 μg ml^{-1}. The bacteria were then cultured in an anaerobic environment at 37 °C for a further 2 h. The OMVs were then collected by ultracentrifugation in a 90-Ti rotor (Beckman) as previously described.

TEM. For negative staining and analysis by TEM, bacteria cultures or concentrated OMVs were allowed to absorb onto freshly glow-discharged Formvar/carbon-coated copper grids for 10 min. The grids were then washed with ddH_2O and stained with 1% phosphotungstic acid for 2 min. Excess liquid was gently blotted off and the grids were air-dried. Samples were examined on a Talos L120C transmission electron microscope.

Quantification of *B. thetaiotaomicron* OMV cargoes. The protein cargo associated with *B. thetaiotaomicron* OMVs was quantified using Qubit protein assay (Invitrogen) by the Qubit 4.0 Fluorometer according to the manufacturer's instructions. For the analysis of OMV-associated DNA or RNA, the OMVs were first incubated with DNase (4 U μl^{-1}) or RNase (10 pg μl^{-1}) at 37 °C for 1 h to degrade extravesicular DNA or RNA, followed by extraction using a minimal DNA and RNA extraction kit (Tiangen). The extracted DNA and RNA were quantified using the Qubit Broad-Range DNA Assay and the Qubit High-Sensitivity RNA Assay, respectively, on a Qubit 4.0 Fluorometer according to the manufacturer's instructions. LPS levels associated with OMVs were quantified using the Limulus Amebocyte Lysate assay (XIAMEN BIOENDO) according to the manufacturer's instructions. Quantification of OMV-associated peptidoglycan was performed as previously described[59]. Briefly, OMV samples and L-18 muramyl dipeptide standards (Invivogen) were diluted to a final volume of 0.5 ml in 1 M NaOH and incubated at 38 °C for 30 min. The reaction was neutralized by adding 0.5 ml of 0.5 M H_2SO_4 and 5 ml of concentrated H_2SO_4, followed by incubation at 95 °C for 5 min. The samples were rapidly cooled under running water, and 50 μl of 4% (w/v) $CuSO_4$ solution and 100 μl of 1.5% (w/v) 4-phenylphenol solution (prepared in 96% ethanol) were added. The mixture was incubated at 30 °C for 30 min, and absorbance was measured at 560 nm using a spectrophotometer. Peptidoglycan content was determined using a standard curve generated with muramyl dipeptide standards.

In vitro DC–IEL–IEC co-culture. DCs and IELs were first sorted by flow cytometry as described above and then resuspended in complete RMPI 1640 growth media (10% v/v FBS, 100 U ml^{-1} penicillin, 100 μg ml^{-1} streptomycin, 10 mM HEPES, 2 mM GlutaMAX, 10 ng ml^{-1} IL-2, 10 ng ml^{-1} IL-3, 10 ng ml^{-1} IL-7, 10 ng ml^{-1} IL-15, and 0.1 μg ml^{-1} anti-CD3ε). DCs and IELs were mixed at a ratio of 1:1 and a total of 200,000 cells were seeded in a round-bottomed 96-well plate. OMVs were added at a final concentration of 4 μg ml^{-1} and co-cultured for 15 h. After careful removal of the culture supernatant, cells were resuspended with fresh complete RMPI 1640 medium and transferred to Transwell filter inserts (0.4-μm pore, Corning), followed by co-culture with pre-seeded primary ileal epithelial cells for 12 h. Cell supernatants from the indicated cell cultures were collected, and then assayed for IFNγ ELISA (R&D Systems) according to the manufacturer's instructions.

Administration of *B. thetaiotaomicron* OMVs. For in vivo OMV reconstitution, mice were orally administered *B. thetaiotaomicron* OMVs (20 μg per 200 μl of PBS) on days 0, 1, 2, 3, 4 and 10, with PBS used as the control. On day 14, the mice were analysed for MHC-II expression and IEL populations, or subjected to *S. typhimurium* infection experiments.

STm infection model. STm strain SL1344 was grown overnight in an LB medium containing streptomycin (100 μg ml^{-1}) and then subcultured (1:100) into a fresh LB medium for 4 h. For survival assays, *Apol9a/b*$^{+/+}$, *Apol9a/b*$^{-/-}$ and *Apol9a/b*$^{-/-}$ mice administered with OMVs were orally infected with 1×10^7 c.f.u. of STm. Mice were monitored throughout the experiment, and mortality was recorded daily. To calculate the bacterial load in the liver and spleen of infected mice,

Apol9a/b$^{+/+}$, *Apol9a/b*$^{-/-}$ and *Apol9a/b*$^{-/-}$ mice administered with OMVs were infected with 1×10^8 c.f.u. of STm by oral gavage, and the liver and spleen were isolated and homogenized on day 5 after infection. Bacterial loads of liver and spleen were determined by plating serial dilutions on LB plates containing streptomycin (100 μg ml^{-1}). In parallel, ileal tissues were collected for histological analysis.

For histopathological analysis, slides were scored blindly by a pathologist at the Department of Gastroenterology, Shanghai Tenth People's Hospital. The overall pathological score was assessed on the basis of five criteria as previously reported[60]: the mucosal thickness, crypt shape and size, spacing between crypts and goblet cell loss.

For systemic infection, mice were injected intraperitoneally with approximately 1×10^4 c.f.u. of the STm strain. Mortality was recorded daily and monitored for 20 d. To assess bacterial burden in the liver and spleen, infected mice were euthanized on day 4 after infection. The liver and spleen were then collected, homogenized in ice-cold PBS, serially diluted and plated on LB agar containing streptomycin to determine c.f.u. counts.

STm infection of IECs. STm infection of primary IECs was performed as previously described with minor modifications[61,62]. Briefly, overnight bacterial cultures were grown in LB medium at 37 °C with shaking for 18 h to the late stationary phase. Cultures were diluted 1:100 in fresh LB medium and incubated to an OD_{600} of 0.6. Bacteria were pelleted by centrifugation, washed twice with PBS and resuspended in complete growth medium (without penicillin/streptomycin) to a concentration of around 5×10^8 c.f.u. per ml. The culture was further serially diluted and added to epithelial cell monolayers at a multiplicity of infection of 10. Plates were centrifuged at 1,000*g* for 5 min to synchronize infection. After 30 min of incubation at 37 °C with 5% CO_2, cells were washed three times with PBS and supplemented with fresh complete growth medium containing 100 μg ml^{-1} gentamicin for 2 h to eliminate extracellular bacteria. The medium was then replaced with a complete growth medium containing 10 μg ml^{-1} gentamicin for the remainder of the experiment. At specified time points, infected cells were lysed with 1% Triton X-100, and intracellular bacteria were enumerated on LB agar plates by c.f.u. analysis.

Statistical analyses

Data are presented as the mean ± s.e.m. Differences between groups were evaluated by ANOVA followed by a Bonferroni post hoc test or by a two-tailed Student's *t*-test with 95% confidence intervals. Survival differences were evaluated by the log-rank (Mantel–Cox) test. To determine the enrichment of certain gene signatures in RNA-seq datasets, we used a Wilcoxon test. *P* values < 0.05 were considered statistically significant. GraphPad Prism 8.0 (v.8.0.0) was used for statistical analysis.

Reporting summary

Further information on research design is available in the Nature Portfolio Reporting Summary linked to this article.

Data availability

The 16S rRNA-seq, bulk RNA-seq and scRNA-seq data generated in this study are available in the NCBI database under BioProject IDs PRJNA1107192, PRJNA1107183, PRJNA1107279, PRJNA1108888 and PRJNA1198673. The public datasets used in this study are available in the NCBI database under the GEO accession numbers GSE92332 and GSE125970 (refs. 27,28). All other data supporting the findings of this study are included in this manuscript. Source data are provided with this paper.

Code availability

No custom code was created for this paper.

47. Garcia-Bayona, L. & Comstock, L. E. Streamlined genetic manipulation of diverse *Bacteroides* and *Parabacteroides* isolates from the human gut microbiota. *mBio* https://doi.org/10.1128/mBio.01762-19 (2019).
48. Sugiura, M. et al. Ceramide kinase, a novel lipid kinase. Molecular cloning and functional characterization. *J. Biol. Chem.* **277**, 23294–23300 (2002).
49. Clarke, E. L. et al. Sunbeam: an extensible pipeline for analyzing metagenomic sequencing experiments. *Microbiome* **7**, 46 (2019).
50. Kang, D. D. et al. MetaBAT 2: an adaptive binning algorithm for robust and efficient genome reconstruction from metagenome assemblies. *PeerJ* **7**, e7359 (2019).
51. Parks, D. H., Imelfort, M., Skennerton, C. T., Hugenholtz, P. & Tyson, G. W. CheckM: assessing the quality of microbial genomes recovered from isolates, single cells, and metagenomes. *Genome Res.* **25**, 1043–1055 (2015).
52. Lam, S. M. et al. A multi-omics investigation of the composition and function of extracellular vesicles along the temporal trajectory of COVID-19. *Nat. Metab.* **3**, 909–922 (2021).
53. Yuan, X. et al. Identification of an endogenous ligand bound to a native orphan nuclear receptor. *PLoS ONE* **4**, e5609 (2009).
54. Han, X., Yang, Y., Zhao, F., Zhang, T. & Yu, X. An improved protein lipid overlay assay for studying lipid-protein interactions. *Plant Methods* **16**, 33 (2020).
55. Couter, C. J. & Surana, N. K. Isolation and flow cytometric characterization of murine small intestinal lymphocytes. *J. Vis. Exp.* https://doi.org/10.3791/54114 (2016).
56. Ivanov, I. I. et al. Induction of intestinal Th17 cells by segmented filamentous bacteria. *Cell* **139**, 485–498 (2009).
57. Hsu, C. C., Okumura, R. & Takeda, K. Human LYPD8 protein inhibits motility of flagellated bacteria. *Inflamm. Regen.* **37**, 23 (2017).
58. Wang, Y. C. et al. Intestinal cell type-specific communication networks underlie homeostasis and response to Western diet. *J. Exp. Med.* https://doi.org/10.1084/jem.20221437 (2023).
59. Gilmore, W. J. et al. *Bacteroides fragilis* outer membrane vesicles preferentially activate innate immune receptors compared to their parent bacteria. *Front. Immunol.* **13**, 970725 (2022).
60. Bousbaine, D. et al. A conserved Bacteroidetes antigen induces anti-inflammatory intestinal T lymphocytes. *Science* **377**, 660–666 (2022).
61. Jiang, L. et al. *Salmonella typhimurium* reprograms macrophage metabolism via T3SS effector SopE2 to promote intracellular replication and virulence. *Nat. Commun.* **12**, 879 (2021).
62. Athman, R. et al. *Shigella flexneri* infection is dependent on villin in the mouse intestine and in primary cultures of intestinal epithelial cells. *Cell. Microbiol.* **7**, 1109–1116 (2005).

Acknowledgements The work received support from the National Key R&D Program of China grant no. 2020YFA0509100, and the NSF of China grant nos. 81830018 and 32030039 (to Y.Q.); the National Key R&D Program of China grant nos. 2022YFA0807300 and 2023YFA1800200, the Strategic Priority Research Program of the Chinese Academy of Sciences (grant no. XDB0990000), the International Partnership Program of the Chinese Academy of Sciences for Future Network (grant no. 318GJHZ2022030FN), the NSF of China grant nos. 32270945 and 92474105, and STCSM grant nos. 22ZR1468700 and 22140902400 (to X.S.); the NSF of China grant nos. 32200036 and 82341116 (to G.L.); and the Department of Defense grant no. HT9425-23-0226 (to D.L.K.). We thank L. Qiu, X. Miao, Y. Bu, Y. Zhai and J. Wu (Institutional Center for Shared Technologies and Facilities of SINH, CAS) for ultracentrifugation and FACS support. We thank Y. Qin, Z. Li and S. Yan (Institutional Center for Shared Technologies and Facilities of SINH, CAS) for technical assistance in microscopy. We appreciate the technical support for lipidomics or lipid structure analysis from LipidALL Technologies (Changzhou, China), Z. Li (Institutional Center for Shared Technologies and Facilities of SINH, CAS) and Z. Yang (Chemical Biology Core Facility of SIBCB, CAS). We also appreciate the technical support for proteomics analysis from PANOMIX Biomedical Tech Co. (Suzhou, China). We thank the staff of the Bioinformatics Core Facility of SIBCB for the scRNA-seq analysis, Y. Kong and L. Pan (Electron Microscopy Core Facilities of ION, CAS) for assistance with EM sample preparation and EM image analysis, and H. Jiang (Core Facility and Technical Service Center for SLSB of SJTU) for technical assistance with FACS analysis of intestinal bacteria. We also thank S. Lin for helping with STm infection experiments (Shanghai Institute of Immunity and Infection, CAS).

Author contributions Y.Q. and X.S. supervised the research. X.S., T.Y., D.L.K. and Y.Q. wrote the manuscript. T.Y. performed proteomics and lipidomics analysis, immunoblotting, immunofluorescence, H&E staining, ceramide kinase assays and bacterial killing assays. T.Y., X.H., F.C. and F.Y. performed flow cytometric sorting of APOL9-binding faecal bacterial taxa and flow cytometric analysis of APOL binding with human gut microbiota. X.H. performed TEM analysis of OMVs and in vitro DC–IEL–IEC co-culture experiments. T.Y. and X.H. performed all sequencing studies and STm infection experiments. F.C. cultured commensal bacterial strains and performed genetic manipulation of *B. thet*. F.Y., M.Z. and G.K. purified recombinant APOL proteins and *B. thet* ceramide kinase. B.N. assisted with immunofluorescence and H&E staining. T.Y., H.Z. and F.C. contributed to the flow cytometry of IELs and LPLs. G.L. and H.G. performed the phylogenetic analysis of the Cer1P biosynthesis genes. K.J., Y.L. and J.S. assisted in the analysis of scRNA-seq data. X.L. performed pathological scoring. T.Y. and M.Z. created all the graphical illustrations for the figures and Extended data figures using Adobe Illustrator CC 2018. D.L.K. and G.H. provided technical assistance and suggestions.

Competing interests The authors declare no competing interests.

Additional information

Supplementary information The online version contains supplementary material available at https://doi.org/10.1038/s41586-025-08990-4.

Correspondence and requests for materials should be addressed to Xinyang Song or Youcun Qian.

Peer review information *Nature* thanks Kenya Honda and the other, anonymous, reviewer(s) for their contribution to the peer review of this work.